

Selenium utilization by GPX4 is required to prevent hydroperoxide-induced ferroptosis --Manuscript Draft--

Manuscript Number:	CELL-D-17-01513R3
Full Title:	Selenium utilization by GPX4 is required to prevent hydroperoxide-induced ferroptosis
Article Type:	Research Article
Keywords:	Ferroptosis, GPX4, Selenoproteins, Selenium, Trsp, Selenocysteine, ACSL4, mouse genetics, glutathione peroxidase
Corresponding Author:	Marcus Conrad Neuherberg, GERMANY
First Author:	Irina Ingold
Order of Authors:	Irina Ingold Carsten Berndt Sabine Schmitt Sebastian Doll Gereon Poschmann Katalin Buday Antonella Roveri Xiaoxiao Peng Florencio Porto Freitas Tobias Seibt Lisa Mehr Michaela Aichler Axel Walch Daniel Lamp Martin Jastroch Sayuri Miyamoto Wolfgang Wurst Fulvio Ursini Elias SJ Arnér Noelia Fradejas-Villar Ulrich Schweizer Hans Zischka José Pedro Friedmann Angeli Marcus Conrad
Abstract:	Selenoproteins are rare proteins among all kingdoms of life containing the 21st amino acid selenocysteine. Selenocysteine resembles cysteine, differing only by the substitution of selenium for sulfur. Yet the actual advantage of selenolate- versus thiolate-based catalysis has remained enigmatic, as most of the known selenoproteins also exist as cysteine-containing homologs. Here, we demonstrate that selenolate-based catalysis of the essential mammalian selenoprotein GPX4 is unexpectedly dispensable for normal embryogenesis. Yet, the survival of a specific type of

	<p>interneurons emerges to exclusively depend on selenocysteine-containing GPX4, thereby preventing fatal epileptic seizures. Mechanistically, selenocysteine utilization by GPX4 confers exquisite resistance to irreversible overoxidation as cells expressing a cysteine variant are highly sensitive towards peroxide-induced ferroptosis. Remarkably, concomitant deletion of all selenoproteins in Gpx4cys/cys cells revealed that selenoproteins are dispensable for cell viability provided partial GPX4 activity is retained. Conclusively, 200 years after its discovery, a specific and indispensable role for selenium is provided.</p>
Opposed Reviewers:	
Suggested Reviewers:	<p>Leopold Flohé, Prof. Dr Otto-von-Guericke-Universität Magdeburg, l.flohe@t-online.de Prof. Flohé is a renowned biochemist and was among the first to identify in 1973 that mammalian glutathione peroxidases are indeed selenoproteins. His work led to landmark contributions in our understanding of the mechanisms of peroxidase catalysis.</p> <p>Vadim Gladyshev Brigham and Women's Hospital, Harvard Medical School vgladyshev@rics.bwh.harvard.edu Prof Gladyshev is a leader in the field of selenoprotein research. His group was responsible for the characterization of the selenoproteome, whereby he then characterized the function and activity for several of these selenoproteins</p> <p>Michel Toledano CEA-Saclay michel.toledano@cea.fr Dr. Michel Toledano is a worldwide expert in the field of redox biology. He has made seminal contributions to our understanding of how hydroperoxides work as signaling molecules and on the enzymes responsible for sensing and responding to this cellular messenger.</p> <p>Brent Stockwell Columbia University bstockwell@columbia.edu Prof Stockwell is a renowned chemical biologist whose work using small molecules targeting specific cancer entities led to the discovery of ferroptosis. Since its discovery his groups has made several important contributions to our understanding of ferroptosis at the molecular level</p> <p>Douglas Green St. Jude Children's Research Hospital douglas.green@stjude.org Prof. Green is an opinion leader in the field of cell death. His group has contributed to our better understanding of cell death both at the molecular level and at the evolutionary level. He has been particularly dedicated in the study of apoptosis, necroptosis and autophagy and their cross-talk with the immune system.</p> <p>Arne Holmgren Karolinska Institutet Arne.Holmgren@ki.se Dr Holmgren is a pioneer in redox biology whose goals are to understand the detailed mechanisms and role of thioredoxin and glutathione-glutaredoxin systems in redox reactions and control of physiological processes. He was responsible for the discovery of the selenoprotein Thioredoxin Reductase.</p>

Helmholtz Zentrum München · P.O. Box 11 29 · 85758 Neuherberg

Sarah Geisler, Ph.D.
Scientific Editor, Cell

Dr. Marcus Conrad

Institute of Developmental Genetics

Phone +49(0)89 3187-4608
Fax +49(0)89 3187-4288
marcus.conrad@helmholtz-muenchen.de

11/16/17

Dear Sarah,

We would like to thank you for the suggestions to finalize our manuscript.

Concerning the individual points required for finalization:

- We removed the duplicate manuscript containing tracked changes and changed the graphical abstract according to the guidelines. The supplemental Movie 1 and "Related to" information had already been included in the main text document in the section "Supplemental Figures".
- Based on our previous publication (Friedmann Angeli et al. 2014), where no sex impact was evidenced on the phenotype induced by Gpx4 loss, we did not systematically analyze the contribution of sex in the current study. Since at present we lack specific information of sex on each individual mouse such a specific analysis is not possible without a new cohort of animals. Therefore, for the sake of clarity we state in the discussion section (last sentence page 14) that the sex contribution was not investigated.
- We provide additional information in the Statistics section defining the value of n and explaining the rationale of statistical analyses.
- We addressed the required changes in the key resource table according to the guidelines.

Enclosed you will find the finalized version of our manuscript "Selenium utilization by GPX4 is required to prevent hydroperoxide-induced ferroptosis" by Ingold *et al.* [CELL-D-17-01513R1].

We look very much forward hearing from you.

Kind regards,

Marcus

Helmholtz Zentrum München
Deutsches Forschungszentrum für
Gesundheit und Umwelt (GmbH)
Ingolstädter Landstr. 1
85764 Neuherberg
Phone +49(0)89 3187 (0)
Fax +49(0)89 3187 3322

info@helmholtz-muenchen.de
www.helmholtz-muenchen.de

Aufsichtsratsvorsitzende:
MinDir'in Bärbel Brumme-Bothe

Geschäftsführer:
Prof. Dr. Günther Wess
Heinrich Baßler
Dr. Alfons Enhsen

Registergericht:
Amtsgericht München HRB 6466
USt-IdNr. DE 129521671

Bankverbindung:
Münchner Bank eG
Konto-Nr. 2 158 620
BLZ 701 900 00
IBAN DE04701900000002158620
BIC GENODEF1M01

No response required

Selenium utilization by GPX4 is required to prevent hydroperoxide-induced ferroptosis

Irina Ingold¹, Carsten Berndt², Sabine Schmitt³, Sebastian Doll¹, Gereon Poschmann⁴, Katalin Buday¹, Antonella Roveri⁵, Xiaoxiao Peng⁶, Florencio Porto Freitas¹, Tobias Seibt⁷, Lisa Mehr¹, Michaela Aichler⁸, Axel Walch⁸, Daniel Lamp^{9,10}, Martin Jastroch^{9,10}, Sayuri Miyamoto¹¹, Wolfgang Wurst^{1,12,13}, Fulvio Ursini⁵, Elias S. J. Arnér¹⁴, Noelia Fradejas-Villar¹⁵, Ulrich Schweizer¹⁵, Hans Zischka^{3,16}, José Pedro Friedmann Angeli^{1,17}, Marcus Conrad^{1,18,*}

1 Helmholtz Zentrum München, Institute of Developmental Genetics, 85764 Neuherberg, Germany

2 Heinrich-Heine University, Department of Neurology, Medical Faculty, 40255 Düsseldorf, Germany

3 Institute of Toxicology and Environmental Hygiene, Technical University of Munich, 80802 Munich, Germany

4 Heinrich-Heine University, Molecular Proteomics Laboratory, Biomedical Research Center (BMFZ), 40225 Düsseldorf

5 Department of Molecular Medicine, University of Padova, Padova, Italy

6 CVMD Translational Medicine Unit, Early Clinical Development, AstraZeneca, Mölndal, Sweden

7 Department of Nephrology, Medizinische Klinik und Poliklinik IV, Klinikum der Universität München, 80336 München, Germany

8 Research Unit of Analytical Pathology, Helmholtz Zentrum München, 85764 Neuherberg, Germany

9 Helmholtz Diabetes Center and German Diabetes Center (DZD), Helmholtz Zentrum München, 85764 Neuherberg, Germany

10 Helmholtz Zentrum München, Institute for Diabetes and Obesity, 85748 Garching, Germany

11 Departamento de Bioquímica, Instituto de Química, Universidade de São Paulo, São Paulo, São Paulo, Brazil

12 German Center for Neurodegenerative Diseases (DZNE), 81377 Munich, Germany

13 Technische Universität München-Weihenstephan, Chair of Developmental Genetics, c/o Helmholtz Zentrum München, 85764 Neuherberg, Germany

14 Division of Biochemistry, Department of Medical Biochemistry and Biophysics, Karolinska Institutet, 171 77 Stockholm, Sweden

15 Rheinische Friedrich-Wilhelms-University Bonn, Institute for Biochemistry and Molecular Biology, 53115 Bonn, Germany

16 Helmholtz Zentrum München, Institute of Molecular Toxicology and Pharmacology, 85764 Neuherberg, Germany

17 Present address: Rudolf Virchow Center for Experimental Biomedicine, University of Würzburg, 97080 Würzburg, Germany

18 Lead Contact

*Correspondence: marcus.conrad@helmholtz-muenchen.de; Tel: +49-89-31874608

SUMMARY

Selenoproteins are rare proteins among all kingdoms of life containing the 21st amino acid selenocysteine. Selenocysteine resembles cysteine, differing only by the substitution of selenium for sulfur. Yet the actual advantage of selenolate- versus thiolate-based catalysis has remained enigmatic, as most of the known selenoproteins also exist as cysteine-containing homologs. Here, we demonstrate that selenolate-based catalysis of the essential mammalian selenoprotein GPX4 is unexpectedly dispensable for normal embryogenesis. Yet, the survival of a specific type of interneurons emerges to exclusively depend on selenocysteine-containing GPX4, thereby preventing fatal epileptic seizures. Mechanistically, selenocysteine utilization by GPX4 confers exquisite resistance to irreversible overoxidation as cells expressing a cysteine variant are highly sensitive towards peroxide-induced ferroptosis. Remarkably, concomitant deletion of all selenoproteins in *Gpx4^{cys/cys}* cells revealed that selenoproteins are dispensable for cell viability provided partial GPX4 activity is retained. Conclusively, 200 years after its discovery, a specific and indispensable role for selenium is provided.

KEYWORDS

Ferroptosis, GPX4, selenoproteins, selenium, Trsp, selenocysteine, ACSL4, mouse genetics, glutathione peroxidase

INTRODUCTION

The trace element selenium (Se) was discovered two centuries ago (in 1817) by the Swedish scientist Jöns Jacob Berzelius (Berzelius, 1818). In biological systems, Se exerts its essential role as the 21st amino acid, selenocysteine (Sec). Sec incorporation, at the opal codon UGA, is a highly complex and energetically costly process (Hatfield et al., 2014). Despite the complexity for Sec usage, it is recognized that Se in form of Sec is indispensable for mammalian life (Bosl et al., 1997). This is supported by the embryonic lethal phenotype of mice deficient for the Sec-specific tRNA gene *Trsp* (*nuclear encoded tRNA selenocysteine 2 (anticodon TCA)*) (Bosl et al., 1997). Since Sec differs from cysteine (Cys) only by the replacement of sulfur for Se and since Cys incorporation presents a canonical translational insertion, the actual biological advantage of selenolate- over thiolate-based catalysis has remained elusive. Remarkably, while some organisms like higher plants and fungi use the readily available sulfur to express Cys-homologs, mammals, fish, birds, nematodes and bacteria still maintain the energetically costly and inefficient process of selenoprotein expression (Lobanov et al., 2007).

Model studies in mice deficient for individual selenoproteins have indicated that the only protein closely mimicking loss of *Trsp* is glutathione peroxidase 4 (GPX4). Constitutive deletion of *Gpx4* causes embryonic death almost at the same developmental stage as *Trsp* knockout mice (Yant et al., 2003). Moreover, tissue-specific knockout approaches unveiled that loss of *Gpx4* alone often phenocopied the effects induced by conditional *Trsp* deletion as demonstrated for certain neurons and epidermis (Sengupta et al., 2010; Wirth et al., 2014; Wirth et al., 2010). In the present work we took advantage of this specific

characteristic of GPX4 and challenged the relevance and importance of selenolate- versus thiolate-based catalysis by generating mice with targeted mutation of the active site Sec to Cys. Data presented herein provide hitherto unrecognized and intriguing insights into the requirement for Se utilization in mice and establish an essential function for GPX4-Sec based catalysis in peroxide-induced ferroptosis prevention.

RESULTS

Selenolate-Based GPX4 Catalysis is Dispensable for Normal Embryogenesis but Essential for the Survival of PV+ Interneurons and Prevention of Seizures

The generation of mice with a targeted mutation of the catalytically active Sec to Cys of GPX4 is depicted in Figures 1A-C. Upon germline transmission, breeding of heterozygous *Gpx4*^{wt/cys} mice was setup to examine whether homozygous *Gpx4*^{cys/cys} mice are viable. Unexpectedly, homozygous *Gpx4*^{cys/cys} mice developed normally and were born at the expected Mendelian ratio (28%) (Table 1). This is in stark contrast to systemic *Gpx4*^{-/-} or *Gpx4*^{ser/ser} (enzymatically inactive) mice, which were both shown to die *in utero* as early as E7.5 (E, embryonic day) (Brutsch et al., 2015; Ingold et al., 2015). Next, GPX4 specific activity in different tissues derived from wildtype (wt) and *Gpx4*^{cys/cys} pups was measured using phosphatidylcholine hydroperoxide (PCOOH) as substrate. Yet, we were unable to detect any GPX4-specific activity in kidney and brain extracts of *Gpx4*^{cys/cys} animals (Figure 1D) (Schneider et al., 2006).

Though *Gpx4^{cys/cys}* mice were born normally (Table 1), homozygous mice appeared to lose body weight by P14-16 (P, postnatal day) (Figure 1E); by P18 all animals had to be sacrificed (Figure 1F). *Gpx4^{cys/cys}* animals showed severe spontaneous seizures or were hyperexcitable (see Supplementary video 1). Since parvalbumin-positive (PV+) GABAergic interneurons are important regulators of cortical network excitability (Mihaly et al., 1997; Schwaller et al., 2004) and mature between P8 and P16, we then asked whether seizures are caused by a lack of these specialized neurons. In fact, staining for parvalbumin (PV) showed a marked decrease of PV+ cells in the cortex of *Gpx4^{cys/cys}* mice (Figure 1G and S1A), whereas the number of calbindin- and calretinin-positive neurons was unaltered (Figure S1B). Along with the decrease of PV+ interneurons an increased number of TUNEL (Terminal deoxynucleotidyl transferase dUTP nick end labeling)-positive cells was detectable in the cortex of *Gpx4^{cys/cys}* mice (Figure 1G and S1A). Cell death coincided with an increased immunohistological staining of glial fibrillary acidic protein and ionized calcium binding adaptor molecule 1, suggestive of reactive astrogliosis and neuroinflammation, respectively (Figure 1G). Hence, GABAergic PV+ interneurons emerge to exclusively depend on Se-containing GPX4, which we identify here to be the limiting factor for survival of mice on a mixed *C57BL/6J* x *129S6SvEv* genetic background.

During backcrossing *Gpx4^{wt/cys}* mice on a *C57BL/6J* background for more than 7-8 generations and subsequent intercross of heterozygous *Gpx4^{wt/cys}* mice, we failed to obtain viable homozygous mutant animals. A ratio of 74% for *Gpx4^{wt/cys}* and 26% for *Gpx4^{wt/wt}* suggested embryonic death of homozygous *Gpx4^{cys/cys}* embryos. Histopathological analysis of embryos isolated at different times of gestation revealed that embryos died between E11.5 and E12.5 (Table S1 and Figure S1C). Overall, mutant embryos showed severe

malformations of the brain, growth retardation, hemorrhages and generalized paleness (Figure S1C and S1D). Crossbreeding of *Gpx4*^{wt/cys} mice (on a *C57BL/6J* background) with *129S6SvEv* wt mice and subsequent intercross of F1 *Gpx4*^{wt/cys} mice allowed to regain the initial phenotype, indicating that the background has a strong impact on the severity of the phenotype of *Gpx4*^{cys/cys} embryos.

Thiolate-Based GPX4 Catalysis Permits Survival of Adult Mice

To bypass early embryonic death or pre-weaning lethality of *Gpx4*^{cys/cys} mice and to address whether the Cys variant of GPX4 (GPX4-Cys) is able to sustain viability in adult mice, we cross-bred *Gpx4*^{wt/cys} mice (and *Gpx4*^{wt/ser} as controls (Ingold et al., 2015)) with mice harboring loxP-flanked (floxed) *Gpx4* alleles and transgenic for Tamoxifen (TAM)-inducible CreERT2 (Friedmann Angeli et al., 2014) (Figure 2A). TAM injection results in whole body deletion of the floxed *Gpx4* allele (except in brain), while still expressing the Cys or the serine (Ser) variant of GPX4. TAM injection caused loss of GPX4 expression in *Gpx4*^{flox/wt;Rosa26_CreERT2} animals to some extent (a gene-dosage effect has been previously reported (Friedmann Angeli et al., 2014; Yant et al., 2003)), whereas expression of mutant GPX4 was maintained in both induced *Gpx4*^{flox/ser;Rosa26_CreERT2} and *Gpx4*^{flox/cys;Rosa26_CreERT2} mice (Figure 2B). Survival analysis revealed that induced *Gpx4*^{flox/ser;Rosa26_CreERT2} mice phenocopied *Gpx4*^{flox/flox;Rosa26_CreERT2} mice leading to mouse lethality ~11 days after TAM administration (Friedmann Angeli et al., 2014) (Figure 2C). By stark contrast, *Gpx4*^{flox/cys;Rosa26_CreERT2} mice survived the entire observation period of 40 days like *Gpx4*^{flox/wt;Rosa26_CreERT2} control mice without showing any signs of kidney damage (Figures 2C,D and S2). *Gpx4*^{flox/ser;Rosa26_CreERT2}

animals, however, died of acute renal failure (ARF) and presented the same histopathological phenotype in kidney as reported for inducible *Gpx4* null mice (Figure 2D) (Friedmann Angeli et al., 2014). These findings demonstrate that Sec of GPX4 can be substituted by Cys in adult animals, whereas Sec appears to be essential during specific developmental events independent of the genetic background.

Generation and characterization of *Gpx4*^{cys/cys} mouse embryonic fibroblasts

Next, we embarked to decipher the biochemical and cellular features that may account for the observed *in vivo* phenotypes. Therefore, mouse embryonic fibroblasts (MEFs) were established as a cellular tool (Figure 3A). All cell lines derived from the different genotypes were viable in cell culture and proliferated normally (Figure 3A). Labeling of selenoproteins with ⁷⁵Se showed the complete lack of ⁷⁵Se incorporation into GPX4 of *Gpx4*^{cys/cys} cells, excluding any unspecific incorporation of Sec into the mutant protein (Figure 3B). Immunoblotting revealed augmented GPX4 expression in *Gpx4*^{cys/cys} cells with an intermediary expression in heterozygous cells (Figure 3C), without detectable changes in mRNA levels (Figure 3D), thus supporting a facilitated co-translational incorporation of Cys. Expression analysis of other important selenoproteins and redox-related enzymes (TXNRD1, TXNRD2, peroxiredoxins-1-3) expressed in cultured cells did not show compensatory upregulation, with the exception of mitochondrial peroxiredoxin-3 (Figure S3). Moreover, as observed in the tissues of *Gpx4*^{cys/cys} animals, GPX4 specific activity was drastically reduced (Figure 3E), hinting towards the possibility that the mutant enzyme could be inactivated by its substrate in the classical GPX4-specific enzyme assay.

***Gpx4^{cys/cys}* Cells are Extremely Sensitive to Peroxide-Induced Cell Death**

Intrigued by the possibility that the enzyme substrate could inactivate the mutant enzyme, we then interrogated the sensitivity of *Gpx4^{cys/cys}* cells to peroxide treatment. In fact, *Gpx4^{cys/cys}* cells presented an unforeseen sensitivity to peroxide-induced cell death when using hydrogen peroxide (H₂O₂), tert-butyl hydroperoxide and cholesterol hydroperoxide (Figure 4A and S4A). Importantly, the mitochondrial complex I inhibitors rotenone and phenformin, which also indirectly contribute to intracellular H₂O₂ formation via superoxide dismutation (Chouchani et al., 2014), provoked similar cell death inducing effects (Figure S4B). Remarkably, this sensitivity was specific to peroxides as *Gpx4^{cys/cys}* cells were equally resistant to other cell stress inducing agents like wt cells (Figure S4C). Of notice, *Gpx4^{cys/cys}* cells were even more resistant to ferroptosis inducing agents (Figure S4D), mainly due to increased GSH levels (Figure S4E), and decreased nucleophilicity of the catalytic thiolate compared to selenolate (Figure S4F) (Yang et al., 2016).

***Gpx4^{cys/cys}* Cells Undergo Peroxide-Induced Ferroptosis**

Next, we performed ultrastructural analysis in order to comprehend the events triggered by peroxide-induced cell death in *Gpx4^{cys/cys}* cells. These studies revealed that *Gpx4^{cys/cys}* cells exposed to H₂O₂ presented the same ultrastructural features like wt cells exposed to the GPX4 inhibitor RSL3, which are loss of mitochondria cristae and outer mitochondrial membrane rupture (Figure S5A). This drastic mitochondrial phenotype, however, could not be accounted for alterations in the expression and functionality of components of the mitochondrial respiratory chain (Figure S5B-I).

Intrigued by this unforeseen sensitivity of *Gpx4*^{cys/cys} cells towards peroxides, we asked which cell death modality is triggered in *Gpx4*^{cys/cys} cells. As illustrated in Figures 4B and 4C, peroxide-induced cell death could be fully rescued in *Gpx4*^{cys/cys} cells by ferroptosis inhibitors (Figures 4B and C) (Conrad et al., 2016), but not by inhibitors targeting other cell death paradigms, such as apoptosis and necroptosis (Figures S6A-C). Notably, H₂O₂-induced cell death in wt cells could not be prevented by any of the aforementioned cell death inhibitors (Figure 4B), indicating that at (extremely) high peroxide concentrations wt cells die in an unspecific, necrotic manner (Friedmann Angeli et al., 2014).

Our previous studies showed that inactivation of GPX4 in cells culminates in phospholipid peroxidation and cell death, which can be blunted by vitamin E and ferroptosis inhibitors (Friedmann Angeli et al., 2014; Seiler et al., 2008). To this end, lipid peroxidation was assessed using BODIPY 581/591 C11. While H₂O₂-treated *Gpx4*^{cys/cys} cells showed a marked increase in oxidation of the dye (Figure 4D), wt cells presented only marginal oxidation. Remarkably, liproxstatin-1 completely suppressed lipid peroxidation as previously reported for *Gpx4*^{-/-} cells (Friedmann Angeli et al., 2014).

Additionally, with the recent recognition that acyl-CoA synthetase long-chain family member 4 (ACSL4) expression determines sensitivity to ferroptosis (Dixon et al., 2015; Doll et al., 2017), we next evaluated its expression levels in *Gpx4*^{cys/cys} and wt cells. As shown in Figure 4E, a marked decrease of ACSL4 expression was detected in *Gpx4*^{cys/cys} cells, suggesting compensatory mechanisms to lower the sensitivity of *Gpx4*^{cys/cys} cells to ferroptosis induction. Supporting this concept, *Gpx4*^{cys/cys} cells showed increased sensitivity towards exogenous treatment with polyunsaturated fatty acids (Figure S6D), while

CRISPR/Cas9-mediated knockout of *Acs14* in GPX4-Cys cells rendered cells more resistant to peroxide-induced cell death (Figure 4F).

GPX4^{cys/cys} is Intrinsically Susceptible to Peroxide-Mediated, Irreversible Overoxidation

To shed light into the striking sensitivity of GPX4-Cys expressing cells towards peroxide-induced cell death, we assessed the redox state of GPX4 using several independent approaches. First, *in situ* dimedone labeling coupled to immunostaining was used to trap the sulfenic acid/selenenic acid intermediate (Klomsiri et al., 2010) (Figure 5A). To this end, FLAG-Strep-HA (FSH)-tagged Cys variant of GPX4 (further referred to as U46C) and FSH-tagged wt GPX4 cells were first treated with dimedone followed by H₂O₂ for the indicated times. A time-dependent increase (~ 5-fold) of dimedone labeling could be detected in GPX4 U46C cells (Figure 5B), whereas almost no labeling was detected in wt GPX4 cells. Mass spectrometry analysis confirmed that upon H₂O₂ treatment, the critical Cys46 of GPX4 was found to be oxidized to sulfonic acid (SO₃H), while under basal conditions this Cys residue of the protein was mostly present in a reduced state and could be detected as an N-ethylmaleimide (NEM) adduct (Figure 5C).

To further assess the dynamics of cysteine oxidation, we used the thiol labeling reagent Methyl-PEG-Maleimide (mm(PEG)24). To avoid "artefactual" labeling, we mutated all nine non-catalytic cysteine residues of GPX4 to Ser (all Cys/Ser Cys), thus allowing us to directly monitor the redox state of the active site. As illustrated in Figure 5D, Cys46 (all Cys/Ser Cys) showed a concentration-dependent decrease in mm(PEG)24 labeling, consistent with GPX4 overoxidation. Moreover, time dependent experiments revealed that the irreversible

oxidation of GPX4 occurred very rapidly, suggesting that the GPX4 mutant protein readily undergoes irreversible oxidation upon increased levels of H₂O₂. Taken together, data from these experiments suggest that in the GPX4-Cys variant overoxidation is readily favored upon exposure to H₂O₂. A scheme summarizing the catalytic cycle of a sulfur-containing GPX4 in the absence or presence of “high” concentrations of peroxides accounting for loss of viability is depicted in Figure 5E.

***Gpx4*^{cys/cys} Cells Proliferate in the Absence of Selenoproteins**

As lack of Se in GPX4 emerges as a critical event in most of the phenotypes observed in mice lacking selenoprotein synthesis, the use of *Gpx4*^{cys/cys} cells (which express GPX4 independently of Se incorporation) would allow us to experimentally challenge this assumption. As such, we decided to target the *Trsp* gene (encoding tRNA^{[Ser]^{Sec}}) (Figure 6A) in cells expressing either the wt or the GPX4-Cys variant (Mannes et al., 2011). To avoid background differences, we first used the isogenic *Gpx4* conditional knockout cell line (PFa1 cells; (Seiler et al., 2008)) for genetic manipulation as described in Figure 6B. In short, cells lacking endogenous GPX4 and expressing Cas9 combined with ectopically expressing wt GPX4 or GPX4-Cys (U46C) were transduced with a virus expressing the *Trsp* guide and a BFP (blue fluorescent protein) marker. After 48h, 100 cells expressing BFP were plated in a cell culture dish in the presence or absence of α -tocopherol (α -Toc). The colony forming assay revealed that *wt GPX4:Trsp*^{mut/mut} formed significantly less colonies in the absence of α -Toc than *U46C:Trsp*^{mut/mut} cells (Figure 6B), suggesting that Se incorporation becomes critical to suppress ferroptosis when cells can only express wt GPX4.

Next, we decided to use the CRISPR/Cas9 approach to delete *Trsp* in *Gpx4*^{wt/wt} and *Gpx4*^{cys/cys} MEFs (stably expressing Cas9) and characterize in detail cells surviving loss of *Trsp* (Figure 6C). Selected cell clones, where both alleles were successfully edited, are depicted in Figure 6C. Sequencing the region targeted by the sgRNA in the selected clones confirmed that a 34 bp deletion was obtained for one allele in both cell lines, while a one bp insertion or deletion at the acceptor arm of tRNA^{[Ser]Sec} resulted in the corresponding *Gpx4*^{wt/wt}:*Trsp*^{-34/+1} and *Gpx4*^{cys/cys}:*Trsp*^{-34/-1} cell lines, respectively. Despite the genetic modifications induced in both *Gpx4*^{wt/wt}:*Trsp*^{-34/+1} and *Gpx4*^{cys/cys}:*Trsp*^{-34/-1} cells, expression of housekeeping selenoproteins expressed in cultured cells, such as GPX4, TXNRD1 and TXNRD2, was still detectable by immunoblotting, albeit at reduced levels (Figure 6D). Since *Gpx4*^{cys/cys}:*Trsp*^{-34/-1} cells express the GPX4-Cys variant, its expression was expected, whereas in case of TXNRD1 and TXNRD2 the remaining proteins likely represent either a truncated form (n.b. Sec is the penultimate amino acid at the C-Terminus of these enzymes), or an unspecific incorporation of Cys as previously described (Xu et al., 2007). Sodium selenite (Na₂SeO₃) supplementation did not increase expression of GPX4 or TXNRD1 in mutagenized cells in contrast to parental cell lines (Figure 6D), suggesting the lack of Se incorporation into these selenoproteins. Metabolic labeling of cells with ⁷⁵Se demonstrated the complete absence of ⁷⁵Se incorporation into selenoproteins of *Gpx4*^{cys/cys}:*Trsp*^{-34/-1} cells (Figure 6E). Yet, in *Gpx4*^{wt/wt}:*Trsp*^{-34/+1} cells Se incorporation in TXNRD1 and GPX4 was still detectable, indicating a residual function of the mutated *Trsp* allele (+1 bp) in *Gpx4*^{wt/wt}:*Trsp*^{-34/+1} cells (Figure 6E), which permits cells to survive.

Treating cells with cytotoxic stimuli showed a further sensitization of *Gpx4*^{cys/cys}:*Trsp*^{-34/-1} cells towards peroxide-induced cell death (Figure 6F). The increased sensitivity of

Gpx4^{cys/cys}:Trsp^{-34/-1} compared to *Gpx4^{cys/cys}* is most likely due to the lack/decreased activity of other selenoproteins involved in the metabolism of H₂O₂ such as TXNRD1/2. In contrast, no differences were observed in *Gpx4^{wt/wt}:Trsp^{-34/+1}* cells versus parental cells when treated with peroxides. Yet, RSL3-treated *Gpx4^{wt/wt}:Trsp^{-34/+1}* cells showed increased sensitivity compared to their parental counterparts (Figure 6F), likely accounting for the lower expression of Se-containing GPX4. Treating cells with the electrophilic TXNRD inhibitor auranofin (Anestal et al., 2008) revealed an increased resistance of *Gpx4^{cys/cys}:Trsp^{-34/-1}* cells (Figure 6F), consistent with the absence of Sec incorporation into TXNRD (see Figure 6E). Conclusively, these findings suggest that cell proliferation and survival do not require selenoproteins as long as a residual GPX4 function is maintained. Moreover, this data reinforce the notion that the phenotypes observed by the complete loss of tRNA^{[Ser]Sec} are, mostly, accounted by the loss of *Gpx4*.

DISCUSSION

Postnatal Interneuron Development Requires Selenium in GPX4

Two hundred years after its discovery by Jöns Jacob Berzelius (Berzelius, 1818), we provide compelling *in vivo* evidence for the advantage of utilizing the trace element Se in form of Sec in GPX4 in mice. By comparing the effects of Cys versus Sec utilization in GPX4, we now show that Sec in GPX4 is indispensable for life. This allowed us to uncover a distinct neuronal cell type, i.e. PV+ interneurons, requiring the presence of Se-containing GPX4. Hence, the specific loss of PV+ interneurons limits the overall survival of homozygous *Gpx4^{cys/cys}* mice due to the development of epileptic seizures. Consistent with the

importance of Se for PV+ interneurons, mice carrying a neuron-specific knockout in the selenoprotein biosynthesis factor *Secisbp2* express very low levels of Sec-containing GPX4, and present significantly reduced numbers of PV+ and glutamic acid decarboxylase-67 (Gad67)-positive interneurons, and die at about the same age as *Gpx4*^{cys/cys} mice (Seeher et al., 2014). Earlier reports have already provided a link between Se status and seizures in man (Ramaekers et al., 1994; Weber et al., 1991), as well as in animal models using Se-deprived rats or conditional knockout for *Trsp*, *SelenoP* and *Gpx4* in mice (Renko et al., 2008; Savaskan et al., 2003; Wirth et al., 2010). A potential explanation for the dependence of PV+ interneurons to wt GPX4 might be their increased metabolic rate, and thus increased basal H₂O₂ production, as these neurons mature after birth and are fast spiking inhibitory neurons reflecting their high demand for ATP (Kann, 2016). Additionally, as neurons contain a high content of polyunsaturated fatty acids (PUFAs), necessary for migration and synapse formation, they are exquisitely sensitive to ferroptosis as recently shown for other cells (Doll et al., 2017). It is also intriguing that homozygous *Gpx4*^{cys/cys} mutant mice survive until 2-3 weeks after birth on a mixed background, while they die during mid-gestation on a *C57BL/6J* congenic background, still considerably later than *Gpx4*^{-/-} embryos. Hence, it seems there must be modifier genes on the different genetic backgrounds that modulate the sensitivity to ferroptosis under specific conditions. This finding might be extrapolated to the human situation as patients suffering from a very rare disease linked to a truncated versions of *GPX4*, called Sedaghatian-type spondylometaphyseal dysplasia (SSMD), also die soon after birth (Smith et al., 2014). Moreover, since we did not observe any sex contribution to the phenotype induced by *Gpx4* loss (Friedmann Angeli et al., 2014), the current study did not assess the contribution of sex to the phenotype observed in the GPX4-Cys mice.

Sec-containing GPX4 Prevents Ferroptosis by its Intrinsic Resistance to Irreversible Inactivation

Having shown the relevance for selenolate-based GPX4 catalysis in distinct developmental processes, we could further demonstrate that the GPX4-Cys variant undergoes overoxidation and irreversible inactivation in the presence of exceeding concentrations of its substrates. This overoxidation seems to be shared with another mammalian selenoprotein, i.e. TXNRD2 (Snider et al., 2013). These findings support the notion that the critical advantage of selenolate- versus thiolate-based catalysis lies in its resistance to overoxidation, a notion that has been previously postulated based on studies using recombinant proteins (Reich and Hondal, 2016). Unlike the wt enzyme, which can form a selenylamide in the absence/low levels of reducing equivalents (GSH), thereby preventing its irreversible overoxidation, the GPX4-Cys fails to form such an intermediate during its catalytic cycle (Orian et al., 2015). The remarkable resistance to peroxide-mediated inactivation emerges to be essential for controlling lipid peroxidation and ferroptosis. While peroxide-induced cell death in wt GPX4 expressing cells appears to involve non-specific, unregulated necrotic cell death (as it could not be prevented by known cell death inhibitors), cells expressing the Cys variant are highly sensitive to ferroptosis triggered by peroxides. Therefore, it is tempting to speculate that the presence of Sec in GPX4 was evolutionary retained in order to accommodate a certain level of cellular peroxides that could be, for instance, exploited for cell signaling purposes without impacting on cell viability (Conrad et al., 2010; Holmstrom and Finkel, 2014; Rhee, 1999). Alternatively, efficient clearance of H₂O₂ and other peroxides generated as by-products during normal cell respiration or during the action of certain cellular enzymes, such as xanthine oxidase, might

require the presence of Sec instead of Cys in the active site of GPX4; a notion reinforced by our finding showing that GPX4-Cys expressing cells are inherently sensitive to mitochondrial complex I inhibitors.

GPX4 is the Limiting Selenoprotein for Mammalian Cell Survival

Beyond the essential role for wt GPX4 to prevent ferroptosis, we also demonstrate that mammalian cells obviously do not require any selenoprotein for proliferation and survival, at least in cell culture, as long as they keep a residual GPX4 activity by expressing the GPX4-Cys variant. Since the majority of selenoproteins expressed in mammalian cells act as oxidoreductases they can be functionally replaced, in most cases, by other redox enzymes. As opposed to this, GPX4 seems to be special as it does not only keep (phospho)lipid hydroperoxides in check but also protects against ferroptosis. And due to this uniqueness, GPX4 cannot be replaced by any of the other redox-active enzymes.

Selenolate-Based Catalysis Allows Enrichment of PUFAs in Membranes

It is also surprising that ACSL4 was found to be downregulated in cells expressing GPX4-Cys. In light of our previous studies that knockout or pharmacological inhibition of ACSL4 causes a strong reduction in the content of PUFAs in membranes (Angeli et al., 2017; Doll et al., 2017; Kagan et al., 2017), decreased expression of ACSL4 in GPX4-Cys cells thus lowers the risk of generating lethal signals of ferroptotic death. Unlike invertebrates, which mainly insert monounsaturated and saturated fatty acids in their lipid bilayers (Haddad et al., 2007;

Shmookler Reis et al., 2011), mammalian lipid bilayers consist of up to 62% of unsaturated fatty acids of which 35% are PUFAs (Hulbert et al., 2002). In fact, Sec utilization of GPX4 is mainly preserved in vertebrates including mammals, fish, birds and amphibians (Figure S7), which form complex brains and predominantly esterify long chain PUFAs in their lipid bilayers (Wallis et al., 2002). PUFAs, which are particularly enriched in brain, liver, testes and kidney (Friedmann Angeli et al., 2014; Hambright et al., 2017), are essential and have afforded an increased repertoire of cellular and physiological functions, such as membrane fluidity, plasticity, neuronal network development, migration and neurotransmitter release (Dickinson et al., 2011), cold adaptation (Cossins and Prosser, 1978), mitochondrial ATP generation (Che et al., 2014), and pathogen defense (Wallis et al., 2002). It is thus provocative to hypothesize that the evolutionary pressure to maintain a Sec-containing GPX4 might correlate with an organism's requirement for an increased PUFA content, which, in turn, renders complex biological activities possible. Yet, the increased functionalization of membranes due to an increase in PUFA content comes with an inherent burden, the intrinsic sensitivity towards lipid peroxidation (Barelli and Antonny, 2016) and ferroptosis.

STAR METHODS

SUPPLEMENTAL INFORMATION

Supplemental Information includes seven figures and two tables.

AUTHOR CONTRIBUTION

Conceptualization, I.I., J.P.F.A. and M.C; Methodology, I.I., J.P.F.A. and M.C; Investigation, I.I. C.B., G.P., S.S., K.B., M.A., X.P., N.F.V., A.R., F.P.F., S.D., D.L., T.S., L.M.; Resources, W.W., H.Z., M.J., A.W., E.S.J.A., U.S. F.U., and S.M.; Writing – Original Draft, I.I., J.P.F.A. and M.C; Writing – Review & Editing, I.I., J.P.F.A. and M.C; Visualization; I.I.; Supervision, M.C., J.P.F.A; Funding Acquisition, W.W., M.C.

ACKNOWLEDGEMENTS

We would like to thank Elena Yefremova and Jonas Wanninger for excellent technical assistance. We would also like to thank Dr. Anton Berns, The Netherlands Cancer Institute, Amsterdam, for providing the *Rosa26-CreER^{T2}* mouse line. This work was in part supported by grants from the Deutsche Forschungsgemeinschaft (DFG) CO 291/2-3 and CO 291/5-1 to M.C., BE3259/5-1 to C.B., Fapesp #13/07937-8, #10/50891-0 to S.M, and the Human Frontier Science Program (HFSP) RGP0013 to M.C and F.U., as well as a Humboldt Postdoctoral scholarship to J.P.F.A.

REFERENCES

- Anestal, K., Prast-Nielsen, S., Cenas, N., and Arner, E.S. (2008). Cell death by SecTRAPs: thioredoxin reductase as a prooxidant killer of cells. *PLoS One* 3, e1846.
- Angeli, J.P.F., Shah, R., Pratt, D.A., and Conrad, M. (2017). Ferroptosis Inhibition: Mechanisms and Opportunities. *Trends Pharmacol Sci* 38, 489-498.
- Barelli, H., and Antonny, B. (2016). Lipid unsaturation and organelle dynamics. *Curr Opin Cell Biol* 41, 25-32.
- Berzelius, J.J. (1818). Undersökning af en ny Mineral-kropp, funnen i de orenare sorterna af det i Falun tillverkade svafvet. *Afhandlingar i fysik, kemi och mineralogi* 6:42.

Bornkamm, G.W., Berens, C., Kuklik-Roos, C., Bechet, J.M., Laux, G., Bachl, J., Korndoerfer, M., Schlee, M., Holzel, M., Malamoussi, A., *et al.* (2005). Stringent doxycycline-dependent control of gene activities using an episomal one-vector system. *Nucleic Acids Res* *33*, e137.

Bosl, M.R., Takaku, K., Oshima, M., Nishimura, S., and Taketo, M.M. (1997). Early embryonic lethality caused by targeted disruption of the mouse selenocysteine tRNA gene (*Trsp*). *Proc Natl Acad Sci U S A* *94*, 5531-5534.

Brinkman, E.K., Chen, T., Amendola, M., and van Steensel, B. (2014). Easy quantitative assessment of genome editing by sequence trace decomposition. *Nucleic Acids Res* *42*, e168.

Brutsch, S.H., Wang, C.C., Li, L., Stender, H., Neziroglu, N., Richter, C., Kuhn, H., and Borchert, A. (2015). Expression of inactive glutathione peroxidase 4 leads to embryonic lethality, and inactivation of the *Alox15* gene does not rescue such knock-in mice. *Antioxidants & redox signaling* *22*, 281-293.

Che, R., Yuan, Y., Huang, S., and Zhang, A. (2014). Mitochondrial dysfunction in the pathophysiology of renal diseases. *Am J Physiol Renal Physiol* *306*, F367-378.

Chouchani, E.T., Pell, V.R., Gaude, E., Aksentijevic, D., Sundier, S.Y., Robb, E.L., Logan, A., Nadtochiy, S.M., Ord, E.N., Smith, A.C., *et al.* (2014). Ischaemic accumulation of succinate controls reperfusion injury through mitochondrial ROS. *Nature* *515*, 431-435.

Conrad, M., Angeli, J.P., Vandenabeele, P., and Stockwell, B.R. (2016). Regulated necrosis: disease relevance and therapeutic opportunities. *Nat Rev Drug Discov* *15*, 348-366.

Conrad, M., Jakupoglu, C., Moreno, S.G., Lippl, S., Banjac, A., Schneider, M., Beck, H., Hatzopoulos, A.K., Just, U., Sinowatz, F., *et al.* (2004). Essential role for mitochondrial thioredoxin reductase in hematopoiesis, heart development, and heart function. *Molecular and cellular biology* *24*, 9414-9423.

Conrad, M., Sandin, A., Forster, H., Seiler, A., Frijhoff, J., Dagnell, M., Bornkamm, G.W., Radmark, O., Hooft van Huijsduijnen, R., Aspenstrom, P., *et al.* (2010). 12/15-lipoxygenase-derived lipid peroxides control receptor tyrosine kinase signaling through oxidation of protein tyrosine phosphatases. *Proc Natl Acad Sci U S A* *107*, 15774-15779.

Cossins, A.R., and Prosser, C.L. (1978). Evolutionary adaptation of membranes to temperature. *Proc Natl Acad Sci U S A* *75*, 2040-2043.

Dalton, A.J. (1955). A chrome-osmium fixative for electron microscopy. *Anat Record* *121*:281.

Dickinson, B.C., Peltier, J., Stone, D., Schaffer, D.V., and Chang, C.J. (2011). Nox2 redox signaling maintains essential cell populations in the brain. *Nature chemical biology* *7*, 106-112.

Dixon, S.J., Winter, G.E., Musavi, L.S., Lee, E.D., Snijder, B., Rebsamen, M., Superti-Furga, G., and Stockwell, B.R. (2015). Human Haploid Cell Genetics Reveals Roles for Lipid Metabolism Genes in Nonapoptotic Cell Death. *ACS Chem Biol* *10*, 1604-1609.

Doll, S., Proneth, B., Tyurina, Y.Y., Panzilius, E., Kobayashi, S., Ingold, I., Irmiler, M., Beckers, J., Aichler, M., Walch, A., *et al.* (2017). ACSL4 dictates ferroptosis sensitivity by shaping cellular lipid composition. *Nature chemical biology* *13*, 91-98.

Fischer, M., Horn, S., Belkacemi, A., Kojer, K., Petrungaro, C., Habich, M., Ali, M., Kuttner, V., Bien, M., Kauff, F., *et al.* (2013). Protein import and oxidative folding in the mitochondrial intermembrane space of intact mammalian cells. *Mol Biol Cell* *24*, 2160-2170.

Friedmann Angeli, J.P., Schneider, M., Proneth, B., Tyurina, Y.Y., Tyurin, V.A., Hammond, V.J., Herbach, N., Aichler, M., Walch, A., Eggenhofer, E., *et al.* (2014). Inactivation of the

ferroptosis regulator Gpx4 triggers acute renal failure in mice. *Nature cell biology* *16*, 1180-1191.

Godoy, J.R., Funke, M., Ackermann, W., Haunhorst, P., Oesteritz, S., Capani, F., Elsasser, H.P., and Lillig, C.H. (2011). Redox atlas of the mouse. Immunohistochemical detection of glutaredoxin-, peroxiredoxin-, and thioredoxin-family proteins in various tissues of the laboratory mouse. *Biochimica et biophysica acta* *1810*, 2-92.

Haddad, L.S., Kelbert, L., and Hulbert, A.J. (2007). Extended longevity of queen honey bees compared to workers is associated with peroxidation-resistant membranes. *Exp Gerontol* *42*, 601-609.

Hambright, W.S., Fonseca, R.S., Chen, L., Na, R., and Ran, Q. (2017). Ablation of ferroptosis regulator glutathione peroxidase 4 in forebrain neurons promotes cognitive impairment and neurodegeneration. *Redox Biol* *12*, 8-17.

Hatfield, D.L., Tsuji, P.A., Carlson, B.A., and Gladyshev, V.N. (2014). Selenium and selenocysteine: roles in cancer, health, and development. *Trends in biochemical sciences* *39*, 112-120.

Hitz, C., Wurst, W., and Kuhn, R. (2007). Conditional brain-specific knockdown of MAPK using Cre/loxP regulated RNA interference. *Nucleic Acids Res* *35*, e90.

Holmstrom, K.M., and Finkel, T. (2014). Cellular mechanisms and physiological consequences of redox-dependent signalling. *Nat Rev Mol Cell Biol* *15*, 411-421.

Hulbert, A.J., Rana, T., and Couture, P. (2002). The acyl composition of mammalian phospholipids: an allometric analysis. *Comp Biochem Physiol B Biochem Mol Biol* *132*, 515-527.

Ingold, I., Aichler, M., Yefremova, E., Roveri, A., Buday, K., Doll, S., Tasdemir, A., Hoffard, N., Wurst, W., Walch, A., *et al.* (2015). Expression of a Catalytically Inactive Mutant Form of Glutathione Peroxidase 4 (Gpx4) Confers a Dominant-negative Effect in Male Fertility. *J Biol Chem* *290*, 14668-14678.

Kagan, V.E., Mao, G., Qu, F., Angeli, J.P., Doll, S., Croix, C.S., Dar, H.H., Liu, B., Tyurin, V.A., Ritov, V.B., *et al.* (2017). Oxidized arachidonic and adrenic PEs navigate cells to ferroptosis. *Nature chemical biology* *13*, 81-90.

Kann, O. (2016). The interneuron energy hypothesis: Implications for brain disease. *Neurobiol Dis* *90*, 75-85.

Klomsiri, C., Nelson, K.J., Bechtold, E., Soito, L., Johnson, L.C., Lowther, W.T., Ryu, S.E., King, S.B., Furdui, C.M., and Poole, L.B. (2010). Use of dimedone-based chemical probes for sulfenic acid detection evaluation of conditions affecting probe incorporation into redox-sensitive proteins. *Methods Enzymol* *473*, 77-94.

Lobanov, A.V., Fomenko, D.E., Zhang, Y., Sengupta, A., Hatfield, D.L., and Gladyshev, V.N. (2007). Evolutionary dynamics of eukaryotic selenoproteomes: large selenoproteomes may associate with aquatic life and small with terrestrial life. *Genome Biol* *8*, R198.

Mandal, P.K., Seiler, A., Perisic, T., Kolle, P., Banjac Canak, A., Forster, H., Weiss, N., Kremmer, E., Lieberman, M.W., Bannai, S., *et al.* (2010). System x(c)- and thioredoxin reductase 1 cooperatively rescue glutathione deficiency. *J Biol Chem* *285*, 22244-22253.

Mannes, A.M., Seiler, A., Bosello, V., Maiorino, M., and Conrad, M. (2011). Cysteine mutant of mammalian GPx4 rescues cell death induced by disruption of the wild-type selenoenzyme. *FASEB J* *25*, 2135-2144.

Mihaly, A., Szente, M., Dubravcsik, Z., Boda, B., Kiraly, E., Nagy, T., and Domonkos, A. (1997). Parvalbumin- and calbindin-containing neurons express c-fos protein in primary and secondary (mirror) epileptic foci of the rat neocortex. *Brain Res* *761*, 135-145.

Moreno-Mateos, M.A., Vejnar, C.E., Beaudoin, J.D., Fernandez, J.P., Mis, E.K., Khokha, M.K., and Giraldez, A.J. (2015). CRISPRscan: designing highly efficient sgRNAs for CRISPR-Cas9 targeting in vivo. *Nat Methods* *12*, 982-988.

Muller, F.L., Liu, Y., Abdul-Ghani, M.A., Lustgarten, M.S., Bhattacharya, A., Jang, Y.C., and Van Remmen, H. (2008). High rates of superoxide production in skeletal-muscle mitochondria respiring on both complex I- and complex II-linked substrates. *The Biochemical journal* *409*, 491-499.

Orian, L., Mauri, P., Roveri, A., Toppo, S., Benazzi, L., Bosello-Travain, V., De Palma, A., Maiorino, M., Miotto, G., Zaccarin, M., *et al.* (2015). Selenocysteine oxidation in glutathione peroxidase catalysis: an MS-supported quantum mechanics study. *Free radical biology & medicine* *87*, 1-14.

Peng, X., Mandal, P.K., Kaminsky, V.O., Lindqvist, A., Conrad, M., and Arner, E.S. (2014). Sec-containing TrxR1 is essential for self-sufficiency of cells by control of glucose-derived H₂O₂. *Cell death & disease* *5*, e1235.

Poschmann, G., Seyfarth, K., Besong Agbo, D., Klafki, H.W., Rozman, J., Wurst, W., Wiltfang, J., Meyer, H.E., Klingenspor, M., and Stuhler, K. (2014). High-fat diet induced isoform changes of the Parkinson's disease protein DJ-1. *J Proteome Res* *13*, 2339-2351.

Ramaekers, V.T., Calomme, M., Vanden Berghe, D., and Makropoulos, W. (1994). Selenium deficiency triggering intractable seizures. *Neuropediatrics* *25*, 217-223.

Reich, H.J., and Hondal, R.J. (2016). Why Nature Chose Selenium. *ACS Chem Biol* *11*, 821-841.

Renko, K., Werner, M., Renner-Muller, I., Cooper, T.G., Yeung, C.H., Hollenbach, B., Scharpf, M., Kohrle, J., Schomburg, L., and Schweizer, U. (2008). Hepatic selenoprotein P (SePP) expression restores selenium transport and prevents infertility and motor-incoordination in Sepp-knockout mice. *The Biochemical journal* *409*, 741-749.

Rhee, S.G. (1999). Redox signaling: hydrogen peroxide as intracellular messenger. *Exp Mol Med* *31*, 53-59.

Rodriguez, C.I., Buchholz, F., Galloway, J., Sequerra, R., Kasper, J., Ayala, R., Stewart, A.F., and Dymecki, S.M. (2000). High-efficiency deleter mice show that FLPe is an alternative to Cre-loxP. *Nat Genet* *25*, 139-140.

Roveri, A., Maiorino, M., and Ursini, F. (1994). Enzymatic and immunological measurements of soluble and membrane-bound phospholipid-hydroperoxide glutathione peroxidase. *Methods Enzymol* *233*, 202-212.

Savaskan, N.E., Brauer, A.U., Kuhbacher, M., Eyupoglu, I.Y., Kyriakopoulos, A., Ninnemann, O., Behne, D., and Nitsch, R. (2003). Selenium deficiency increases susceptibility to glutamate-induced excitotoxicity. *FASEB journal : official publication of the Federation of American Societies for Experimental Biology* *17*, 112-114.

Schmitt, S., Saathoff, F., Meissner, L., Schropp, E.M., Lichtmannegger, J., Schulz, S., Eberhagen, C., Borchard, S., Aichler, M., Adamski, J., *et al.* (2013). A semi-automated method for isolating functionally intact mitochondria from cultured cells and tissue biopsies. *Anal Biochem* *443*, 66-74.

Schmitt, S., Schulz, S., Schropp, E.M., Eberhagen, C., Simmons, A., Beisker, W., Aichler, M., and Zischka, H. (2014). Why to compare absolute numbers of mitochondria. *Mitochondrion* 19 Pt A, 113-123.

Schneider, M., Vogt Weisenhorn, D.M., Seiler, A., Bornkamm, G.W., Brielmeier, M., and Conrad, M. (2006). Embryonic expression profile of phospholipid hydroperoxide glutathione peroxidase. *Gene Expr Patterns* 6, 489-494.

Schulz, S., Schmitt, S., Wimmer, R., Aichler, M., Eisenhofer, S., Lichtmanegger, J., Eberhagen, C., Artmann, R., Tookos, F., Walch, A., *et al.* (2013). Progressive stages of mitochondrial destruction caused by cell toxic bile salts. *Biochimica et biophysica acta* 1828, 2121-2133.

Schwaller, B., Tetko, I.V., Tandon, P., Silveira, D.C., Vreugdenhil, M., Henzi, T., Potier, M.C., Celio, M.R., and Villa, A.E. (2004). Parvalbumin deficiency affects network properties resulting in increased susceptibility to epileptic seizures. *Molecular and cellular neurosciences* 25, 650-663.

Seeher, S., Atassi, T., Mahdi, Y., Carlson, B.A., Braun, D., Wirth, E.K., Klein, M.O., Reix, N., Miniard, A.C., Schomburg, L., *et al.* (2014). Secisbp2 is essential for embryonic development and enhances selenoprotein expression. *Antioxidants & redox signaling* 21, 835-849.

Seiler, A., Schneider, M., Forster, H., Roth, S., Wirth, E.K., Culmsee, C., Plesnila, N., Kremmer, E., Radmark, O., Wurst, W., *et al.* (2008). Glutathione Peroxidase 4 Senses and Translates Oxidative Stress into 12/15-Lipoxygenase Dependent- and AIF-Mediated Cell Death. *Cell Metab* 8, 237-248.

Sengupta, A., Lichti, U.F., Carlson, B.A., Ryscavage, A.O., Gladyshev, V.N., Yuspa, S.H., and Hatfield, D.L. (2010). Selenoproteins are essential for proper keratinocyte function and skin development. *PLoS One* 5, e12249.

Shmookler Reis, R.J., Xu, L., Lee, H., Chae, M., Thaden, J.J., Bharill, P., Tazearslan, C., Siegel, E., Alla, R., Zimniak, P., *et al.* (2011). Modulation of lipid biosynthesis contributes to stress resistance and longevity of *C. elegans* mutants. *Aging (Albany NY)* 3, 125-147.

Smith, A.C., Mears, A.J., Bunker, R., Ahmed, A., MacKenzie, M., Schwartzenruber, J.A., Beaulieu, C.L., Ferretti, E., Consortium, F.C., Majewski, J., *et al.* (2014). Mutations in the enzyme glutathione peroxidase 4 cause Sedaghatian-type spondylometaphyseal dysplasia. *J Med Genet* 51, 470-474.

Snider, G.W., Ruggles, E., Khan, N., and Hondal, R.J. (2013). Selenocysteine confers resistance to inactivation by oxidation in thioredoxin reductase: comparison of selenium and sulfur enzymes. *Biochemistry* 52, 5472-5481.

Telorack, M., Meyer, M., Ingold, I., Conrad, M., Bloch, W., and Werner, S. (2016). A Glutathione-Nrf2-Thioredoxin Cross-Talk Ensures Keratinocyte Survival and Efficient Wound Repair. *PLoS Genet* 12, e1005800.

Tietze, F. (1969). Enzymic method for quantitative determination of nanogram amounts of total and oxidized glutathione: applications to mammalian blood and other tissues. *Anal Biochem* 27, 502-522.

Wallis, J.G., Watts, J.L., and Browse, J. (2002). Polyunsaturated fatty acid synthesis: what will they think of next? *Trends in biochemical sciences* 27, 467.

Weber, G.F., Maertens, P., Meng, X.Z., and Pippenger, C.E. (1991). Glutathione peroxidase deficiency and childhood seizures. *Lancet* 337, 1443-1444.

Wirth, E.K., Bharathi, B.S., Hatfield, D., Conrad, M., Brielmeier, M., and Schweizer, U. (2014). Cerebellar hypoplasia in mice lacking selenoprotein biosynthesis in neurons. *Biol Trace Elem Res* 158, 203-210.

Wirth, E.K., Conrad, M., Winterer, J., Wozny, C., Carlson, B.A., Roth, S., Schmitz, D., Bornkamm, G.W., Coppola, V., Tessarollo, L., *et al.* (2010). Neuronal selenoprotein expression is required for interneuron development and prevents seizures and neurodegeneration. *FASEB J* 24, 844-852.

Xu, X.M., Carlson, B.A., Mix, H., Zhang, Y., Saira, K., Glass, R.S., Berry, M.J., Gladyshev, V.N., and Hatfield, D.L. (2007). Biosynthesis of selenocysteine on its tRNA in eukaryotes. *PLoS Biol* 5, e4.

Yang, W.S., Kim, K.J., Gaschler, M.M., Patel, M., Shchepinov, M.S., and Stockwell, B.R. (2016). Peroxidation of polyunsaturated fatty acids by lipoxygenases drives ferroptosis. *Proc Natl Acad Sci U S A* 113, E4966-4975.

Yant, L.J., Ran, Q., Rao, L., Van Remmen, H., Shibatani, T., Belter, J.G., Motta, L., Richardson, A., and Prolla, T.A. (2003). The selenoprotein GPX4 is essential for mouse development and protects from radiation and oxidative damage insults. *Free Radic Biol Med* 34, 496-502.

FIGURES

Figure 1. *Gpx4*^{cys/cys} Mice Develop Normally but Fail to Survive the Pre-Weaning Age

(A) Gene targeting strategy for the targeted conversion of Sec to Cys in *Gpx4*. In the upper line, the wildtype (wt) allele of *Gpx4* with the critical exon 3 highlighted in red is shown. In the lower part, the targeting vector used to generate the point mutation in exon 3, where the UGA codon (marked with an asterisk) is located, is shown. For homologous recombination in F1 embryonic stem (ES) cells, the neomycin phosphotransferase gene (*neo*) and thymidine kinase gene (*TK*) were used as positive and negative selection marker, respectively (Abbreviation: BS, pBluescript vector backbone).

(B) ES cell with homologous recombination (HR) of the targeting construct were identified by long range PCR spanning the 3' arm. Germline transmission (GT) of the targeted allele was confirmed by PCR from ear punch DNA (one representative clone out of 25 is shown).

(C) Sequencing of the region covering the critical exon 3 confirmed the targeted mutation in the active site of *Gpx4* (UGA → UGC) in mice heterozygous and homozygous for the targeted *Gpx4* allele (for each genotype one representative chromatogram is shown).

(D) GPX4-specific activity was undetectable in tissues derived from *Gpx4*^{cys/cys} animals using PCOOH as substrate (data represent mean ± s.d. of n = 3 tissues per genotype; statistical analysis was conducted using two-tailed t test ***P*<0.01).

(E) *Gpx4*^{cys/cys} animals were normal in appearance but tended to loose body weight between P14-P16 (P = postnatal day) (data represent mean ± s.d. of n = 3 animals per genotype).

(F) *Gpx4^{cys/cys}* animals died due to sudden death or had to be sacrificed as they suffered from severe spontaneous epileptic seizures (see Supplemental Video 1). They failed to survive beyond the third week after birth (Kaplan Meyer: Statistical survival analysis was conducted using Mantel-cox test **** $P < 0.0001$, $n = 13$ (*Gpx4^{wt/wt}*), 39 (*Gpx4^{wt/cys}*) or 23 (*Gpx4^{cys/cys}*) animals).

(G) Immunohistological analysis of brain obtained from *Gpx4^{cys/cys}* mice and *Gpx4^{wt/wt}* littermates at the age of 16 days after birth (P16) revealed the presence of terminal deoxynucleotidyl transferase dUTP nick end labeling (TUNEL)-positive cells in cortex of homozygous mutant mice, which were absent in wt samples. While parvalbumin-positive (PV+) interneurons were dramatically decreased in *Gpx4^{cys/cys}* animals, they showed an increase in glial fibrillary acidic protein (GFAP) and ionized calcium-binding adapter molecule 1 (IBA1) staining, indicating reactive astrogliosis and microglia activation, respectively (one representative staining is shown of 5 brain tissues per genotype; scale bar = 10 μ m). See also Figure S1A.

Figure 2. Survival of Adult Animals Requires just the Cys Variant of GPX4

(A) Breeding scheme describing the mating steps of *Gpx4^{wt/cys}* or *Gpx4^{wt/ser}* with a mouse strain expressing a loxP-flanked *Gpx4* allele and a Tamoxifen (TAM)-inducible Cre recombinase under the control of the *Rosa26* locus (*Gpx4^{fl/fl};Rosa26_CreERT2*), further referred to as *Gpx4^{fllox/ser;Rosa26_CreERT2}*, *Gpx4^{fllox/cys;Rosa26_CreERT2}* and *Gpx4^{fllox/wt;Rosa26_CreERT2}* mice.

(B) Analysis of GPX4 expression in kidney tissues derived from *Gpx4^{fllox/ser;Rosa26_CreERT2}*, *Gpx4^{fllox/cys;Rosa26_CreERT2}* and *Gpx4^{fllox/wt;Rosa26_CreERT2}* animals revealed decreased protein levels

in *Gpx4*^{flox/wt;Rosa26_CreERT2} and to some extent in *Gpx4*^{flox/ser;Rosa26_CreERT2} kidneys as compared to *Gpx4*^{flox/cys;Rosa26_CreERT2} mice. Analysis was performed 11 days after TAM administration (one representative experiment is shown of 3 replicates).

(C) A Kaplan-Meier analysis showed that *Gpx4*^{flox/ser;Rosa26_CreERT2} animals died between 9 and 12 days after TAM injection, whereas *Gpx4*^{flox/cys;Rosa26_CreERT2} survived like control *Gpx4*^{flox/wt;Rosa26_CreERT2} animals (statistics was assessed using Mantel-cox test *****P*<0.0001, *n* = 7 (*Gpx4*^{flox/wt;Rosa26_CreERT2} and *Gpx4*^{flox/ser;Rosa26_CreERT2}) and 6 (*Gpx4*^{flox/ser;Rosa26_CreERT2}) animals).

(D) Immunohistochemical staining of kidneys after TAM injection showed clear signs of ARF in *Gpx4*^{flox/ser;Rosa26_CreERT2} animals as shown by proteinaceous casts (arrows) in kidney tubules and a strong increase in TUNEL+ staining. Staining against GPX4 indicated decreased expression in *Gpx4*^{flox/ser;Rosa26_CreERT2} animals, which is in line with the immunoblot analysis. Although cell death was strongly increased in *Gpx4*^{flox/ser;Rosa26_CreERT2} kidney, no increase for active caspase-3, a marker for apoptosis, was found (one representative staining is displayed out of 7 *Gpx4*^{flox/ser;Rosa26_CreERT2} and *Gpx4*^{flox/wt;Rosa26_CreERT2} and 6 *Gpx4*^{flox/cys;Rosa26_CreERT2} mice; scale bars upper panel = 20 μm; scale bar other panels =100 μm).

Figure 3. Proliferation of *Gpx4*^{cys/cys} Cells is Indistinguishable from that of wt Cells

(A) Mouse embryonic fibroblasts (MEFs) isolated from embryos from a breeding of heterozygous *Gpx4*^{wt/cys} mice were genotyped by two independent PCRs, yielding a product of 256 bp for wt and 203 bp for the mutated *Gpx4* allele. No differences were obtained in

the proliferation rates of MEFs expressing either the Cys or Sec variant of GPX4 (n = 3 cell clones per genotype).

(B) Supplementation of cells with radioactively labeled ^{75}Se confirmed that *Gpx4*^{cys/cys} MEFs do not unspecifically incorporate Selenium (Se) in the mutant GPX4 protein.

(C) GPX4 protein levels were significantly higher in MEFs heterozygous and homozygous for the Cys variant as compared to wt cells (western blot shows 1 representative experiment performed 3 times).

(D) *Gpx4* mRNA levels were comparable between the different genotypes (n = 3 cell clones per genotype).

(E) Substantially lower GPX4-specific activity was detected in *Gpx4*^{cys/cys} cells compared to *Gpx4*^{wt/cys} or *Gpx4*^{wt/wt} cells using PCOOH as a substrate (data represent the mean of \pm s.d. of n = 3 per genotype. Statistics was assessed using one-way Anova $P < 0.05$ (*); $P < 0.01$ (**); $P < 0.0001$ (****); n.s. = not significant; a.u. = arbitrary unit (A, C, D, E)).

Figure 4. Peroxide-Induced Cell Death of *Gpx4*^{cys/cys} Cells is Ferroptotic

(A) Hydrogen peroxide (H_2O_2) and tert-butyl hydroperoxide (tBOOH) elicited cell death in *Gpx4*^{cys/cys} MEFs already at low concentrations, while in wt cells substantially higher concentrations were needed to obtain the same cell death-inducing effects.

(B) The ferroptosis inhibitors ferrostatin-1 and liproxstatin-1 prevented cell death induced by H_2O_2 in homozygous *Gpx4*^{cys/cys} cells, but not in wt cells.

(C) Low concentrations of liproxstatin-1 blocked cell death in *Gpx4^{cys/cys}* cells even at high H₂O₂ concentrations unlike in wt cells (data represent the mean \pm s.d. of n = 3 wells from 1 representative experiment performed independently 4 times (A, B, C)).

(D) Lipid peroxidation as assessed by BODIPY581/591 staining of cells was not detectable in *Gpx4^{wt/wt}* MEFs treated with low (100 μ M) or even high (750 μ M) H₂O₂ concentrations for 1 h. By contrast, *Gpx4^{cys/cys}* cells showed strong lipid peroxidation already at low H₂O₂ concentrations (100 μ M – 1 h), which could be fully blunted by liproxstatin-1 (1 μ M – 30 min) (one representative experiment out of 3 performed independently is shown).

(E) Western blot analysis revealed that acyl-CoA synthetase long chain family member 4 (ACSL4) was robustly downregulated in *Gpx4^{cys/cys}* cells compared to wt cells (shown is one representative experiment performed 2 times independently. Statistics was determined using two-tailed t test ** $P < 0.01$).

(F) CRISPR/Cas9-mediated knockout (ko) of *Acs4* in cells expressing a FSH-tagged Cys variant of GPX4 (further referred to as U46C) led to a higher resistance of the cells towards H₂O₂ and tBOOH treatment compared to parental cells (data represents the mean \pm s.d. of n = 3 wells from 1 representative experiment performed independently 3 times).

Figure 5. The Cys Variant of GPX4 is Highly Sensitive Towards Overoxidation *In Vivo*

(A) Scheme of sulfenic acid trapping by dimedone.

(B) *In situ* labeling of FSH-wt GPX4 and U46C cells with dimedone and subsequent treatment with 100 μ M H₂O₂ for the indicated times followed by immunoprecipitation revealed

strongly increased dimedone-labeling of the GPX4-Cys protein (at 120 min H₂O₂: mean = 5.13, ± s.e.m.= 1.34; shown is one representative experiment out of 6). In contrast, only marginal dimedone-binding was detected in FSH-tagged wt GPX4 cells (at 120 min H₂O₂: mean = 1.56, ± s.e.m. = 0.23; shown is one representative experiment out of 5).

(C) For mass spectrometry analysis, U46C cells were either incubated with N-ethylmaleimide (NEM) or with H₂O₂ (100 μM – 3h) and NEM prior to cell lysis and protein isolation via immunoprecipitation. Mass spectrometric analysis identified sulfonic acid of C46 in the active site of GPX4 (presented spectrum: precursor charge: 2+, Monoisotopic m/z: 849.895, precursor mass deviation: -0.22ppm, Mascot Ionscore: 93) occurring predominantly under H₂O₂ treated conditions, whereas under basal conditions, C46 was primarily found to be alkylated by NEM (presented spectrum: precursor charge: 2+, Monoisotopic m/z: 888.426, precursor mass deviation: -0.11ppm, Mascot Ionscore: 88). Quantitative analysis of mass spectrometric data revealed a 31-fold increase in intensity of the C46 sulfonic acid peptide variant upon H₂O₂ treatment (data represents mean ± s.d. of n = 3 independent replicates, statistical analysis was performed using two-tailed t test *P<0.05).

(D) Shift analysis experiment using high molecular alkylating experiments. *Gpx4* ko cells (PFa1) ectopically expressing a GPX4 variant with all nine Cys residues being mutated to Ser and the active site Sec to a Cys (all Cys/Ser Cys) were either treated with increasing concentrations of H₂O₂ for 5 min or with a fixed concentration of H₂O₂ (100 μM) for the indicated times. Upon cell lysis, TCEP treatment and alkylation with Methyl-PEG-Maleimide Reagent (mm(PEG)24) immunblotting against GPX4 revealed that as little as 50 μM H₂O₂ was sufficient to irreversibly oxidise the mutant GPX4 protein within 5 min (upper). This oxidation emerged to be very fast because 1 min treatment with 100 μM H₂O₂ was sufficient

to cause irreversible overoxidation (UM = unmodified control; one representative experiments independently performed 3 times is shown).

(E) Scheme illustrating the catalytic cycle of sulfur-containing variant of GPX4 in the presence or absence of high concentrations of peroxides.

Figure 6. CRISPR/Cas9-mediated Deletion of *Trsp* is Possible only in *Gpx4^{cys/cys}* Cells

(A) Cloverleaf model of wt tRNA^{[Ser]_{Sec}.}

(B) Scheme describing the generation of *wt GPX4:Trsp^{mut/mut}* and *U46C:Trsp^{mut/mut}* cells in a PFa1 isogenic background. PFa1 cells stably expressing Cas9 were transduced with virus expressing FSH-tagged wt or U46C GPX4 and selected by TAM administration. Subsequently, cell lines expressing either wt or U46C variants were stably transduced with an sgRNA targeting *Trsp*. Colony forming assays performed right after CRISPR/Cas9-mediated deletion of *Trsp* in FSH-tagged wt GPX4 and U46C cells in the presence and absence of 1 μ M α -Tocopherol (α -Toc) demonstrated a significantly decreased number of *wt GPX4:Trsp^{mut/mut}* colonies formed without α -Toc supplementation in contrast to *U46C:Trsp^{mut/mut}* colonies (data presents the mean \pm s.d. of n = 3; statistics was assessed using two-tailed t test $**P < 0.01$. One representative experiment out of 3 is shown).

(C) Chromatogram showing CRISPR/Cas9-mediated gene alterations of the *Trsp* gene identified in *Gpx4^{wt/wt}:Trsp^{-34/+1}* and *Gpx4^{cys/cys}:Trsp^{-34/-1}* cell lines as compared to wt *Trsp*. *Gpx4^{wt/wt}:Trsp^{-34/+1}* cells contained a 34 bp deletion at the 3' terminus of one allele and a one

bp insertion at position G⁷¹ in the second allele (acceptor arm). In *Gpx4^{cys/cys}:Trsp^{-34/-1}* cells, a 34 bp deletion was also observed on one allele and the deletion of G⁷¹ on the second allele.

(D) Immunoblotting of selenoproteins expressed in cells revealed a decreased expression of housekeeping selenoproteins GPX4, TXNRD1 and TXNRD2 and an absence of the stress-related selenoprotein GPX1 in *Gpx4^{wt/wt}:Trsp^{-34/+1}* cells. As expected, expression of the Cys variant of GPX4 in *Gpx4^{cys/cys}:Trsp^{-34/-1}* cells was unaltered compared to their parental cells. Yet, expression of GPX1, TXNRD1 and TXNRD2 was found to be decreased as well in *Gpx4^{cys/cys}:Trsp^{-34/-1}* cells. In both CRISPR/Cas9 mutagenized gene cell lines Na₂SeO₃ supplementation did not stimulate selenoprotein expression in contrast to their parental counterparts (one representative experiment out of 3 is shown).

(E) ⁷⁵Se labeling demonstrated a complete loss of Se incorporation only in *Gpx4^{cys/cys}:Trsp^{-34/-1}* cells, whereas in *Gpx4^{wt/wt}:Trsp^{-34/+1}* cells only a decrease of Se incorporation into GPX4 and TXNRD1 was detectable.

(F) Peroxide treatment of cells revealed an increased sensitivity only in *Gpx4^{cys/cys}:Trsp^{-34/-1}* (and not in *Gpx4^{wt/wt}:Trsp^{-34/+1}*) cells compared to their parental cell lines. *Gpx4^{wt/wt}:Trsp^{-34/+1}* cells were slightly more sensitive towards RSL3 than the parental cell line. Treatment with auranofin revealed an increased resistance of *Gpx4^{cys/cys}:Trsp^{-34/-1}* cells, likely resulting from the lack of Sec incorporation into TXNRD (data represent the mean ± s.d. of n = 3 wells from one representative experiment performed independently 4 times).

Table 1. Genotyping of Mice Obtained from Heterozygous *Gpx4*^{cys/wt} Breedings

wt/wt	wt/cys	cys/cys	total
25 (20.8%)	61 (50.8 %)	34 (28.3%)	120

Homozygous pups of heterozygous *Gpx4*^{cys/wt} breeding were born at the expected Mendelian ratio.

STAR METHODS

KEY RESOURCES TABLE

CONTACT FOR REAGENT AND RESOURCE SHARING

Further information and requests for reagents may be directed to, and will be fulfilled by the Lead Contact, Marcus Conrad (marcus.conrad@helmholtz-muenchen.de).

EXPERIMENTAL MODEL AND SUBJECT DETAILS

Mice

All mice were bred and maintained in the animal facility of the Helmholtz Zentrum München under SPF-IVC standard conditions with water and food ad libitum and in a controlled environment ($22 \pm 2^\circ\text{C}$, $55 \pm 5\%$ humidity, 12 h light/dark cycle). Cages were supplied with nesting material and houses in case of breeding cages. Mice were grouped with their littermates in 2-5 animals per cage. Offspring was separated from the mothers between days 19-21 after birth and marked by ear punch for identification and genotyping. For embryonic analysis pregnant *Gpx4^{wt/cys}* females (*C57BL/6J* – F8) were used at embryonic day E9.5 - E12.5 after gastrulation. For the remaining experiments both male and female animals were used. Experiments with (*C57BL/6J* × *129S6SvEvTac*) animals were performed at the age of P10 - P16 days. 4-OH-tamoxifen (TAM) injections were performed with animals at the age of 8 - 16 weeks. Littermates of the same genotype were assigned to the corresponding experimental group. All experiments conducted on the animals were in compliance with the German Animal Welfare Law and have been approved by the institutional committee on animal experimentation and the government of Upper Bavaria.

Primary Cells

Primary mouse embryonic fibroblasts (MEFs) were established from embryos at E13.5 after gastrulation from a heterozygous *Gpx4*^{wt/cys} breeding as previously described (Conrad et al., 2004). Cells were cultured in Dulbecco's modified Eagle's medium (DMEM) supplemented with 10% fetal bovine serum (FBS), 1% L-glutamine and 1% penicillin/streptomycin. Primary MEFs were cultured in a 37°C incubator with humidified atmosphere of 5% O₂ and 5% CO₂ (Binder) until passage 15. From passage 15 onwards primary MEFs were defined as immortalized and were then maintained in a 37°C incubator with humidified atmosphere of 20% O₂ and 5% CO₂ (Binder). Sex of primary MEFs is not available.

PFa1, HEK293T Cells and Embryonic Stem Cells

TAM-inducible *Gpx4*^{fl/fl} (fl, floxed = loxP-flanked) cells (further referred to as PFa1 cells) (Seiler et al., 2008) and HEK293T cells were cultured in standard DMEM medium like immortalized MEFs. The PFa1 cell line is male. Embryonic stem (ES) cells (IDG3.2-rosa26 (Hitz et al., 2007)) were cultured on gelatine coated cell plates in Standard DMEM containing sodium pyruvate, 15% FCS, 24 µM HEPES, 1 × MEM nonessential amino acids, 120 µM β-mercaptoethanol and leukemia inhibitory factor (LIF) (1.8 × 10³ U/ml). ES cells were maintained in a 37°C incubator with humidified atmosphere of 20% O₂ and 5% CO₂ (Binder). Sex of ES cells is not available.

METHOD DETAILS

Generation of Mice Expressing Cys-GPX4

To generate mice expressing the cysteine variant of *Gpx4* (further referred to as *Gpx4*^{cys/cys} mice), a targeting vector was designed taking advantage of the two vectors pPNT4.1 and pPNT4.8 that were previously used for generating conditional *Gpx4* knockout mice (Seiler et al., 2008). Both vectors were digested with *AscI* and *SbfI*, whereby the smaller fragment of 4435 bp containing the wildtype (wt) sequence of *Gpx4* from pPNT4.8 was cloned into the backbone of pPNT4.1, yielding the vector pPAF-1. To insert the targeted mutation, two independent PCRs were performed using the “*AscI* forward” primer (5'-AGGAAGGCGCGCCCTCGCCGGAT-3') and a reverse primer containing the mutation for Cys-*Gpx4* (rev: 5'-TCAGTTTTGCCGCATTGCGAGGCCACGT-3'). For the second PCR, a forward primer containing the mutation for Cys-*Gpx4* (fwd: 5'-ACGTGGCCTCGCAATGCGGCAAACTGA-3') and the “*SbfI* reverse” primer (5'-CTTCCTGGCTCCTGCAGGAAGCAAC-3') were used. Two PCR products were obtained spanning either exons 2 to 3 or exons 3 to 4 of the *Gpx4* gene, respectively, partially overlapping in exon 3. The resulting PCR products were used for an overlap PCR using the “*AscI* forward” and the “*SbfI* reverse” primers. The resulting PCR product carrying the mutation was cloned into pDrive (Qiagen) and further transferred in the pPAF1 vector using *AscI* and *SbfI*. The targeting vector was linearized by *Sall* and used for homologous recombination in embryonic stem (ES) cells (cell line IDG3.2-rosa26 established from (C57BL/6J × 129S6SvEvTac)-F₁ blastocysts (Hitz et al., 2007)) as previously described (Ingold et al., 2015). After electroporation 150 clones were isolated, individually expanded and analyzed for homologous recombination using the long range PCR primers “Neo_2 forward”

(5'-GCGATGCCTGCTTGCCGAATATCAT-3') and "Neo_2 reverse" (5'-TTGCTACAATCATGGGCCAGACGGA-3'). Homologous recombination of the targeting vector was observed in 25 out of 150 individually isolated ES cell clones. To check for the correct insertion, ES cell clones were sequenced using primers "oGpx4_mut forward" (5'-CATGGTCTGCCTGGATAAGTACAGGT-3') and "oGpx4_mut reverse" (5'-CTTGGAAGATACTACTACTGTACTACTG-3'). One positive ES cell clone was microinjected into oocytes of BDF mice and transferred into pseudopregnant *CD1* mice (in-house breeding). One chimeric mouse was backcrossed with *C57BL/6J* animals (in-house breeding) for germline transmission. Germline transmission was confirmed by PCR in four out of 15 pups. The genotyping of the pups was conducted by two independent PCRs that either identify the wt allele or the transgenic (tg) allele. For the wt allele the primers "Gpx4_1 forward" (5'-GTTTAAGGATGGTGGTAACCTGCTAG-3') and "Gpx4_3 reverse" (5'-ACTTAGCCCATAGTCCTAAGATCAC-3') were used amplifying a product of 256 bp in size. In case of the transgenic allele the primer "Gpx4_2 forward" (5'-GTGGTATCATTTCAGCTTTGAGAAT-3') and "Gpx4_4 reverse" (5'-CTCCCCTACCCGGTAGAATTAGCTTG-3') were used amplifying a band of 203 bp in size.

Generation of Cells Expressing tagged GPX4

The cDNA sequence of a Flag-Strep-HA (FSH)-tagged variant of *Gpx4* containing a conversion Sec → Cys (further referred to as U46C) was ordered as GeneArt® String™ (Invitrogen). The sequence was codon-optimized for protein production. Gibson cloning was performed according to manufacturer's instructions in order to clone the cDNA sequence into a 442-PL1-IRES-puro (a kind gift from Prof. Dr. Timm Schroeder, ETH Zurich). The 442-PL1-IRES-

puro vector was digested with *Bst*bl and *Xba*l and the cDNA was amplified with primers “442_Gpx4” (fwd: 5'-CGGTCTGAATCAAGCTTATCGATACCGTCGACGGATCCTTGGATCCACTAGTAACGGC-3'; rev: 5'-TACGTAACCGGTCTCGAGACGCGTTCTAGAGAATTCTTCGTCTAGAGCTAGCCTAGGC- 3') to add ~40 bp homology to each end of the digested vector. PFa1 cells were transduced with the cloned plasmid and with a vector containing FSH-tagged wt GPX4 (further referred to as GPX4 wt) (Mannes et al., 2011). Endogenous *Gpx4* was deleted by administration of 1 μ M TAM, thereby selecting cells expressing the exogenous FSH-tagged addback or U46C. The cells were maintained under TAM selection for at least 1 week. Deletion of endogenous GPX4 was confirmed by immunoblotting.

Viral Transduction

Viral transduction was performed using third generation lentiviral vectors (pLentiCas9-Blast, 442-PL1-IRES-puro and pKLV-U6gRNA(BbsI)-PGKpuro2ABFP based vectors) together with the third generation packaging system consisting of pEcoEnv-IRES-puro, pMDLg_pRRE and pRSV_Rev (Kind gift from Prof. Timm Schroeder, ETH Zurich (Seiler et al., 2008)). HEK293T cells were used as packaging system for the production of replication-incompetent ecotropic viral particles. HEK293T cells were seeded to reach 70% confluency after overnight incubation. Cells were co-transfected with one of the transfer vectors and the vectors from the packaging system in a fixed molar ratio (5:2:10:5; total 10 μ g DNA) by mixing vector DNA with X-tremeGene HP DNA Transfection reagent in a ratio of 1:3 (DNA : reagent). 72 h after transfection supernatant containing ecotropic lentiviral particles was collected from the HEK293T cells and sterile filtered using a 45 μ m low protein binding syringe filter. Target

cells were trypsinized and seeded on 6-well plates containing a 1:1 dilution of the infectious supernatant supplemented with 8 µg/ml protamine sulfate to enhance lentiviral transduction. Selection with the corresponding antibiotics started 48 h after transduction.

Doxycycline-Dependent Expression of tagged GPX4

FSH-tagged Cys-Gpx4 DNA sequence (GeneArt® String™, Invitrogen) was cloned into the pRTS1 vector (Bornkamm et al., 2005) using Gibson Cloning method according to manufacturer's instructions. Therefore, the cDNA sequence was amplified with primers "pRTS1_Gpx4" (fwd: 5'- CCTCCGCGGCCCGAATTCCTGCAGATTTAAATACTAGTGGATCCCCGCGGTTCC AACTAGTAACGGCCGCCAGTG-3'; rev: 5'- CATGTCTGGATCCTCTAGAACTAGGTCGACAGATCTTCTAGAGCTAGCCTAGGC-3') containing ~40 bp homology to each end of the pRTS1 vector. PFa1 cells were transfected with the cloned vector (further referred to as Dox U46C) and a pRTS1-FSH-tagged wildtype GPX4 vector (further referred to as Dox wt) (Mannes et al., 2011) by lipofection using the X-tremeGene HP DNA Transfection Reagent. To this end, 200 µl of FCS-free DMEM was mixed with 2 µg plasmid DNA and X-tremeGene HP DNA Transfection Reagent in a ratio of 1:3 (DNA:reagent). The solution was applied dropwise to 5×10^4 cells on a 6-well plate. MEFs were incubated for 72 h before initiating the selection with hygromycin (250 µg/ml final) on a 15 cm cell culture plate. Cells were selected at least for three weeks under the selection of 1 µM TAM and 250 µg/ml hygromycin in the presence of 1 µg/ml doxycycline (Dox). The expression of the Dox-inducible GPX4 proteins was checked by Western blot analysis.

Determination of Cell Proliferation Rates

Cells were seeded on a 24-well plate in four replicates and cell number was determined with the Neubauer chamber using the Trypan blue exclusion method every 24 h by counting for 96 h.

Cell Viability Assay

For testing sensitivity of cells towards different (oxidative) stress inducing agents, cells were seeded on a 96-well plate (2000 cells/well) and treated with increasing concentrations of different compounds ((1*S*,3*R*)-RSL3, tert-butyl hydroperoxide [tBOOH], cholesterol hydroperoxide [ChOOH], H₂O₂, menadione, antimycin A, rotenone, phenformin, myxothiazol, carbonyl cyanide-4-(trifluoromethoxy)phenylhydrazone [FCCP], irinotecan, vinoblastine, mitoxantrone, nocodazol, phenylarsine oxide [PAO] sulforaphane and auranofin). For cell death inhibitor studies, cells were pre-incubated for 2 h with cell death inhibitors α -Tocopherol (α -Toc), necrostatin-1(S), ferrostatin-1, liproxstatin-1, ciclopirox olamine and Z-VAD-FMK before cell death was induced by the aforementioned compounds. After 48-72 h of incubation, cell viability was assessed by AquaBluer (MultiTarget Pharmaceuticals, LLC) fluorescent measurement at 562 nm according to manufacturer's instructions using the SpectraMax plate reader (Molecular Device GmbH) (Friedmann Angeli et al., 2014).

Determination of Lipid Peroxidation

Cells (1×10^5) were seeded on a 10 cm plate and treated with H₂O₂ (for 1 h) alone or in the presence of liproxstatin-1 (30 min). Cells were washed twice and incubated for 15 min with 1 μ M C11-BODIPY (581/591) (Invitrogen). Afterwards, cells were trypsinized, washed twice

and resuspended in phosphate-buffered saline (PBS). Lipid peroxidation was assessed by measuring the fluorescence change of C11-BODIPY (581/591) by flow cytometry using BD FACS Canto II (BD Bioscience) in at least 10,000 cells. Data analysis was conducted using the FlowJo software.

CRISPR/Cas9-Mediated Knockout of *Acs14* and *Trsp*

Knockout of *acyl-CoA synthetase long chain family member 4 (Acs14)* and *nuclear encoded tRNA selenocysteine 2 (anticodon TCA) (Trsp)* in the different MEF cell lines using single guide RNAs and CRISPR/Cas9 technology was conducted as described before (Doll et al., 2017). In brief, single guide RNAs were designed using the platform <http://www.crisprscan.org/> (Moreno-Mateos et al., 2015) and cloned into the ecotropic lentiviral pKLV-U6gRNA(Bbs1)-PGKpuro2ABFP vector (Addgene) using *BbsI* restriction sites. Before transducing cells with the pKLV-U6gRNA-PGKpuro2ABFP vector carrying the CRISPR target sequence, immortalized MEFs were transduced with ecotropic lentiviral particles carrying the pLentiCas9-Blast construct (Addgene). Two days after transduction, positive cells were selected with 10 µg/ml blasticidin (Invitrogen) for 7 days. Blasticidin-resistant cells were used for another transduction with ecotropic lentiviral particles containing the sgRNA of interest expressing plasmid (pKLV-U6gRNA-PGKpuro2ABFP). Two days after transduction, positive cells were selected with 2.5 µg puromycin for two weeks. After selection, cells were seeded at very low cell densities and single cell colonies were allowed to form. Single cell clones were picked and analyzed for the mutations in the corresponding gene using PCR and sequence validation. CRISPR/Cas9 mediated deletion/insertion was

detected using the TIDE: Tracking of Indels by DEcomposition online tool (Brinkman et al., 2014).

Cloning and Sequencing of PCR Products

To analyze the CRISPR/Cas9-induced modifications of the *Trsp* gene in *Gpx4^{wt/wt};Trsp^{-34/+1}* and *Gpx4^{cys/cys};Trsp^{-34/-1}* cells, a PCR of the *Trsp* gene using “Trsp (fwd)” (5`-GGCGCTATGCAAATGAAGCTAC-3`) and Trsp (rev) (5`-GAGCCGGAGTGAACAAATGAACA-3`) primers was performed and PCR products were purified using the Wizard® SV Gel and PCR Clean-Up System (Promega) according to manufacturer`s instructions. The PCR products were then cloned into pDrive vector using a Qiagen PCR cloning kit (Qiagen) according to manufacturer`s instructions. DH5α chemically competent *E.coli* bacteria were transformed with the plasmids. Individual bacterial colonies were used for DNA isolation using QIAprep Spin Miniprep Kit (Qiagen) according to manufacturer`s instructions. DNA was sequenced by GATC Biotech AG (Konstanz).

CRISPR/Cas9 Colony Forming Assay

PFa1 cells were stably transduced with pLentiCas9-Blast (Addgene) and selected for stable Cas9 expression with 10 µg/ml blasticidin. Then, these cells were transduced with 442-puro-FSH-tagged wt Gpx4 or 442-puro-FSH-tagged cys Gpx4 variant (U46C) and selected by TAM administration resulting in the loss of endogenous *Gpx4*. Both cell lines were then transduced with ecotropic lentiviruses expressing the *Trsp* sgRNA (pKLV-U6Trspguide-PGKpuro2aBFP). 48 h after viral transduction BFP (blue fluorescent protein)-positive cells were identified by flow cytometry. Right thereafter, 100 cells per cell line were seeded on a

15 cm cell culture dish with and without additional supplementation of 1 μ M α -tocopherol. Cells were allowed to grow until they formed colonies in Standard DMEM for approximately 10 days. The medium was discarded and cells were washed twice with PBS. Colonies were fixed and stained by methylene blue staining solution (0.2% methylene blue in a solution of 50% H₂O and 50% methanol) for 15 min. Staining solution was discarded and plates were rinsed with dH₂O in order to remove residual staining solution. Plates were finally air-dried and colony numbers were determined by counting.

Determination of mRNA Expression

RNA isolation was performed with the RNeasy Mini Kit according to manufactures' instructions (Qiagen). Total RNA was utilized for cDNA synthesis using Reverse Transcription system Kit (Promega) as described in the manufactures' protocol. cDNA was used for quantitative Real-Time PCR (Abiprism 7900-HT sequence detective system, Applied Biosystems) using either gene-specific TaqMan probes or specific primers in a SYBR green reaction to determine mRNA levels. To this end, TaqMan[®] gene expression assay was conducted according to manufactures' instructions (Applied Biosystems). *Gpx4*-specific primers containing a Fam dye-labeled MGB probe (Applied Biosystems) or primers specific for mitochondrial encoded 12S RNA (*MT-RNRN1*) (AB Applied Biosystems) along with housekeeping control *hypoxanthin-phosphoribosyl-transferase-1* (*Hprt1*)-specific primers containing a Vic dye-labeled MGB-probe in the same reaction (AB Applied Biosystems) were included. Data was analyzed and quantified using the SDS RQ Manager software (Applied Biosystems). The following primers were used to determine kidney damage parameters: *Kidney injury molecule-1* (*Kim-1*) (fwd: 5'-TCAGCTCGGGAATGCACAA-3'; rev: 5'-

TGGTTGCCTTCCGTGTCTCT-3`); *tissue inhibitor of metalloproteinase 2 (Timp-2)* (fwd: 5`- CAGACGTAGTGATCAGAGCCAAA-3`; rev: 5`- ACTCGATGTCTTTGTCAGGTCC-3`), *insulin-like growth factor binding protein 7 (Igfbp7)* (fwd: 5`- AAGAGGCGGAAGGTAAAGC-3`; rev: 5`- TGGGGTAGGTGATGCCGTT-3`) and *18SRNA* (fwd: 5`-GCAATTATTCCCCATGAACG-3`; rev: 5`- AGGGCCTCACTAAACCATCC-3`) as housekeeping control.

Tissue and Embryo Dissection

Female animals from heterozygous *Gpx4^{wt/cys}* breedings were daily checked for vaginal mucous plug. Plug-positive animals were sacrificed at various embryonic (E) stages (E9.5-E12.5) for the isolation of decidua from the uterus. Embryos were either isolated from the decidua for whole mount analysis or were placed in 4% paraformaldehyde (PFA) for immunohistological analysis. For the isolation of tissues, animals were sacrificed either by decapitation or cervical dislocation and organs like brain, thymus, heart, lung, spleen, kidney and liver were dissected and briefly washed in PBS when necessary.

Protein Analysis from Cells and Tissues

Freshly dissected tissues were homogenized with a Eurostar RW16 stirrer in lysis buffer (0.5% Triton-X-100, 0.5% sodium deoxycholate salt, 150 mM NaCl, 20 mM Tris/HCl, 10 mM EDTA, 30 mM sodium pyrophosphate, 1 % protease and 1% phosphatase inhibitor cocktail (both Roche)). Cells were directly lysed in lysis buffer and scraped from the plate with a cell scraper. To remove cell debris, samples were centrifuged at 21,130 × g at 4°C for 15 min. After centrifugation, supernatant was transferred to a new tube. Protein concentration of lysates was determined using the BCA Protein Assay Kit (Thermo Fisher Scientific) according

to manufacturers' description. For immunoblot analysis protein samples (20 µg protein/lane) were separated on a 12% sodium dodecyl sulfate polyacrylamide gel (SDS-Page) and transferred afterwards onto a PVDF membrane (both BioRad). Proteins were probed with GPX4- (1:1000, Abcam), ACSL4- (1:200, Santa Cruz), TXNRD1- (1:3 (Telorack et al., 2016)), TXNRD2- (1:1 (Mandal et al., 2010)), GPX1- (1:1000, Abcam), PRX2 (1:1000, Kind gift from Dr. Lillig), PRX1 and PRX3 (1:1000, (Godoy et al., 2011)) and β-actin-specific antibodies (1:10000, Sigma). HRP conjugated secondary antibodies (Santa Cruz) and the ChemiDoc Imaging System (BioRad) were used to visualize the protein/primary antibody complexes.

Hematoxylin and Eosin Staining (H&E)

Paraffin-embedded tissues were cut in 8 µm-thick sections. After deparaffinization and hydration, sections were stained with Mayer's Hematoxylin (Roth) for 7 min, briefly washed in water and incubated in tap water for 5 min. Sections were again briefly washed in water and stained for 3 min in 0.5% eosin with a drop of glacial acetic acid. After a short washing step with water, sections were dehydrated in a graded series of ethanol (70%, 96% and 100%), treated with xylol and mounted in Roti-Histo Kit (Carl Roth GmbH).

Transmission Electron Microscopy (TEM)

2×10^4 cells were seeded on a 12-well plate and treated for defined times or left untreated. Cells were collected by trypsinization. Cell pellets were fixed in 2.5% electron microscopy grade glutaraldehyde in 0.1 M sodium cacodylate buffer pH 7.4 (Science Services), postfixed in 2% aqueous osmium tetroxide (Dalton, 1955) dehydrated in gradual ethanol (30–100%)

and propylene oxide, embedded in Epon (Merck) and cured for 48 hours at 60°C. Semithin sections were cut and stained with toluidine blue. Ultrathin sections of 50 nm were collected onto 200 mesh copper grids, stained with uranyl acetate and lead citrate before examination by TEM (Zeiss Libra 120 Plus, Carl Zeiss NTS GmbH). Pictures were acquired using a Slow Scan CCD-camera and iTEM software (Olympus Soft Imaging Solutions).

Immunohistochemistry

Freshly dissected tissues were embedded in paraffin and prepared for immunohistochemistry staining as described previously (Ingold et al., 2015). Paraffin-embedded tissues were cut in 8 µm-thick sections and incubated with Calbindin- (1:1000, Swant), Calretinin- (1:2000, Swant), GPX4- (1:250, Abcam) and active Caspase 3-specific antibodies (1:200, Cell Signaling) overnight at 4°C. Detection of staining was achieved by using biotinylated secondary antibody IgG (anti-rabbit 1:200, or anti-mouse 1:250 Vector Laboratories Inc.) and an Avidin-Biotin-Peroxidase Complex (Vectastain ABC kit, Vector Laboratories Inc.) to enhance the signals. 3,3'-diaminobenzidine (DAB, Vector Laboratories Inc.) staining solution was used for visualization of the antibody-peroxidase complexes.

For immunofluorescence staining, freshly dissected tissues were fixed overnight in 4% PFA, followed by an overnight incubation in 20% sucrose if required and embedded in Tissue Tek® (Sakura) mounting medium on dry ice and stored at -80°C. The frozen tissue was cut in 20 µm thick sections at a Kryostat Microm HM 560 (Thermo Fisher Scientific) and stored at -80°C until further processing. Frozen sections were thawed at room temperature and fixed in two steps in 1% paraformaldehyde and afterwards in 100% ethanol:acetic acid (2:1), blocked in blocking solution and incubated over night with antibodies against parvalbumin

(PV) (1:1000, Swant), ionized calcium-binding adapter molecule 1 (IBAI) (1:500, Genetex) and glial fibrillary acidic protein (GFAP) (1:200, Cell Signaling). Fluorescence-labelled secondary antibodies (Alexa fluor 594 anti-mouse or Alexa Fluor 488 anti-rabbit, both Thermo Fisher Scientific) were used for visualization of the signals on an Olympus confocal microscope IX81 (Olympus) using filters 405, 488, 595 nm.

Staining of Dead Cells

Cryo-conserved brain and paraffin-embedded tissues were prepared as aforementioned. Staining of TUNEL-positive cells was performed using either the ApopTag Fluorescein In Situ Apoptosis Detection Kit or the ApopTag Peroxidase In Situ Apoptosis Detection Kit according to the manufacturer's instructions (Merck-Millipore).

Measurement of Kidney Functional Parameters

In order to analyze kidney functional parameters, blood samples were taken from *Gpx4^{flox/cys;Rosa26_CreERT2}* and *Gpx4^{flox/wt;Rosa26_CreERT2}* animals 40 days after TAM administration. Blood samples were centrifuged (4°C, 10 min, 8000 rpm) and blood serum was isolated for further measurements. For detecting kidney function parameters, blood creatinine levels were measured using Creatinine FS Set (DiaSys) according to manufacturer's protocol and blood urea nitrogen levels were measured using Urea FS Kit (DiaSys) according manufacturer's protocol.

Determination of GPX4-Specific Activity

Frozen cell pellets were homogenized in 0.1 ml of homogenizing buffer (HB: 0.1 M $\text{KH}_2\text{PO}_4/\text{K}_2\text{HPO}_4$, 0.15 M KCl, 0.05% (w/v) CHAPS, pH 7.4, containing 5×10^{-3} M 2-mercaptoethanol and a cocktail of protease inhibitors) by 50 pestle strokes in a Dounce tissue grinder and centrifuged at $17,000 \times g$ for 20 min. Frozen tissue samples were grinded in a mortar in the presence of liquid nitrogen to a fine powder. The tissue powder was thoroughly resuspended in 0.2 ml of HB and centrifuged as for cells. Protein concentration in supernatants was measured by the Bradford method using BSA as standard. Fifty microliters of supernatant containing 0.03 ± 0.01 and 0.49 ± 0.19 mg protein for cells and tissues, respectively, were used for activity measurements.

Samples were incubated for 5 min at room temperature in 1 ml of 0.1 M $\text{KH}_2\text{PO}_4/\text{K}_2\text{HPO}_4$, pH 7.8 containing 5 mM EDTA, 5 mM GSH, 0.1% (v/v) Triton X-100, 160 μM NADPH/ H^+ and 180 IU/ml glutathione reductase (GR). Enzymatic activity was triggered by adding 25 μM phosphatidylcholine hydroperoxide (PCOOH) and quantified as the decrease of absorbance at 340 nm due to NADPH/ H^+ oxidation by GR, as reported (Roveri et al., 1994). GPX4-specific activity was expressed as nmoles/min/mg.

Determination of Total Intracellular GSH

Cells were seeded on 6-well plates (1×10^5) and incubated overnight. On the next day, cell culture medium was discarded, and cells were washed twice with ice-cold PBS. 5% trichloroacetic acid (TCA) was applied to the cells to allow permeabilization of the membrane and the release of small molecules including glutathione. Solution was collected in a tube and treated with ether to remove TCA. The assessment of total glutathione level is

based on the catalytic activity of glutathione to reduce 5,5'-dithiobis(2-nitrobenzoic acid) (DTNB) to 2-nitro-5-thiobenzoate (TNB⁻) at the expense of NADPH/H⁺ (Tietze, 1969). To this end, 500 μ l sample was mixed with 1.2 ml assay buffer, 4 mg/ml DNTP, 1 IU GR and 3.62 mg/ml NADPH/H⁺. The total glutathione content is defined by the intensity of the color change from DTNB to TNB⁻ within a period of 5 min at 412 nm absorbance. To calculate total glutathione content per mg protein, cells were treated after TCA extraction with 0.5 M NaOH overnight to solve cellular proteins. Protein quantification was performed using the Pierce BCA Protein Assay Kit (Thermo Fisher Scientific) as described in manufacturer's protocol.

Labeling of primary MEFs with ⁷⁵Se

⁷⁵Se-radioisotope labeling was performed as described previously (Peng et al., 2014), with minor modifications. Cells were seeded and incubated with 1 μ Ci/ml ⁷⁵Se-labeled selenite (Research Reactor Center, University of Missouri) for 48 h. Proteins of clarified supernatants of cell lysates were subsequently fractionated on reducing SDS-PAGE (buffers, gel and equipment from Invitrogen) and transferred onto nitrocellulose membrane using iBlot Dry Blotting System (Thermo Fisher Scientific). Ponceau S staining was used to visualize total protein. The membrane was thereafter exposed to a phosphor screen and autoradiography was finally visualized with a Typhoon FLA 7000 (GE Healthcare Life Sciences).

Labeling of *Trsp* Knockout Cells with ⁷⁵Se

Confluent cell plates, seeded on the day before, were labeled overnight using 10 μ Ci/plate of radioactive sodium selenite (Na₂SeO₃). After labeling, media was removed and plates

were washed twice with 1 x cold PBS. Cell lysates were collected in RIPA buffer (50 mM Tris-HCl (pH 7.5), 150 mM NaCl, 1% NP-40, 0.25% sodium deoxycholate, 1 mM DTT and protease inhibitors) and quantified by BCA method (Thermo Fisher Scientific). 25 µg of protein extract were electrophoresed in a SDS-PAGE gel. The gel was stained with Coomassie brilliant blue to show equal loading. After drying, the gel was exposed for one day to a Phosphoimager screen, which was developed by a BAS-1800 II Phosphoimager (Fujifilm).

Redox State Analysis of GPX4 using Dimedone

For Western blot-based detection of sulfenic acid (-SOH), 70% confluent cells ($2-6 \times 10^6$ cells expressing FSH-tagged wt GPX4 and $1-2 \times 10^6$ cells expressing FSH-tagged GPX4 U46C) were first treated with 5 mM dimedone right before the H₂O₂ challenge. Then, cells were treated for the indicated times (15/30/60/120 min) with 100 µM H₂O₂, thus capturing freshly forming sulfenic acids in the GPX4 protein. For detection of sulfonic acid (-SO₃H) by mass spectrometry, 70% confluent cells were treated with 100 µM H₂O₂ for 180 min. Cells were washed in PBS containing 100 mM N-ethylmaleimide (NEM) and lysed in 50 mM Tris-HCl (pH 7.4) buffer containing 150 mM NaCl, 0.5% Nonidet-P40, 100 mM NEM and protease inhibitor (Roche). GPX4 was isolated using 200 µg of anti-flag M2 magnetic beads (Sigma). SDS-PAGE was performed with Mini-Protean-TGX-gels (BioRad) and Western transfer via the Trans Blot Turbo system (BioRad). Dimedone and GPX4 were visualized by self-made antibodies and secondary antibodies purchased from Li-Cor (IRDye-800CW, IRDye-680RD) and an odyssey infrared scanner (Li-Cor). For GPX4 we used an HA-specific antibody (1:5, Roche).

For the generation of a dimedone-specific antibody, CGC peptide was coupled to lysine residues of ovalbumin and the conjugate reacted with 2-Bromodimedone. The resulting dimedone-modified protein was used for the immunization of rabbits (Pineda) and antibodies affinity purified from antisera before applied for Western Blot analysis. Intensity of signals was quantified using Image J.

Redox State Analysis of the Active Site of GPX4

In order to analyze the redox state of the active site of the GPX4-Cys variant, PFa1 cells were stably transduced with a lentivirus expressing the GPX4-Cys variant with all nine Cys, except the active site, mutated to a Ser (further referred to as all Cys/Ser Cys (Mannes et al., 2011)). The experiment was performed as described previously (Fischer et al., 2013) with minor modifications. Cells were seeded on 10 cm cell culture plates and allowed to reach 80% confluency before the H₂O₂ challenge. Cells were either treated in a concentration- (1/10/50/100 μM for 5 min) or time-dependent (1/3/5/10 min with 100 μM) manner with H₂O₂. One cell plate was left untreated as a control. Cell culture medium was removed after treatment, and cells were washed twice with ice cold PBS, lysed in 8% ice-cold TCA (trichloroacetic acid) and were frozen at -20°C overnight. On the following day, the protein samples were thawed at room temperature and precipitated proteins were washed once with 5% ice-cold TCA and 3 times with ice-cold acetone. The protein pellet was resuspended in 90 μl non-reducing 1 × Laemmli buffer by sonication at 50°C until they were completely dissolved. Dissolved samples were diluted 1:10 in 30 μl 1 × Laemmli buffer and boiled at 95°C for 10 min in the presence of 1% SDS. Afterwards, samples were incubated with 2 mM tris(2-carboxyethyl)phosphine (TCEP) for 15 min at 95°C in order to reduce reversibly

oxidized cysteines. Finally, protein samples were modified for 2 h using the alkylation agent Methyl-PEG-Maleimide Reagent (mm(PEG)24; Thermo Fisher Scientific) (final concentration 12 mM) at room temperature in the dark, whereby one control sample was left unmodified. Proteins were separated by electrophoresis in a 12% SDS-PAGE and transferred on a nitrocellulose membrane by wet transfer. The unmodified and labelled GPX4 protein was visualized using a GPX4-specific antibody and HRP-conjugated secondary antibodies.

Mass Spectrometry Analysis of GPX4

Immunoprecipitation of GPX4 was performed and eluates were separated by SDS PAGE as described above. GPX4 containing bands were excised and processed with a few modifications as described recently (Poschmann et al., 2014). Three samples per group were individually processed and measured. Briefly, samples were washed, alkylated as a control for yet unreacted cysteines with 55 mM iodoacetamide in a 50 mM ammonium hydrogen carbonate containing aqueous solution, digested with 0.066 µg trypsin (Serva) in a 100 mM ammonium hydrogen carbonate containing aqueous solution overnight at 37°C. Resulting peptides were extracted from the gel with 1:1 (v/v) 0.1 % trifluoroacetic acid (TFA) / acetonitrile and after vacuum concentration resuspended in 34 µl 0.1 % TFA and analyzed with liquid chromatography coupled electrospray ionization mass spectrometry. Here, peptides were separated on an UltiMate 3000 RSLCnano chromatography system (Thermo Fisher Scientific). Initially, peptides were pre-concentrated on a 2 cm long trap column (Acclaim PepMap100, 3 µm C18 particle size, 100 Å pore size, 75 µm inner diameter, Thermo Fisher Scientific) for 10 min at a flow rate of 6 µl/min with 0.1 % (v/v) TFA as mobile phase. Subsequently, they were separated on a 25 cm long analytical column (Acclaim

PepMapRSLC, 2 μm C18 particle size, 100 \AA pore size, 75 μm inner diameter, Thermo Fisher Scientific) at 60°C using a 54 min gradient from 4 to 40% solvent B (solvent A: 0.1 % (v/v) formic acid in water, solvent B: 0.1 % (v/v) formic acid, 84 % (v/v) acetonitrile in water) at a flow rate of 300 nl / min. The amount of solvent B was increased to 95 % within one minute and held at 95 % for additional 4 min. Separated peptides were analyzed with a Q Exactive plus hybrid quadrupole-orbitrap mass spectrometer (Thermo Fisher Scientific) coupled to the liquid-chromatography system via a nano electrospray ionization source equipped with distal coated SilicaTip emitters (New Objective). The instrument was operated data-dependently in positive mode; the spray voltage was between 1.4 and 1.8 kV and the capillary temperature between 250 and 275°C. First, survey scans were recorded in the orbitrap in profile mode over a mass range from 200 – 2000 m/z at a resolution of 70000 (at 400 m/z) with the target value for automatic gain control set to 3000000 and the maximum ion time to 50 ms. Second, up to twenty > 1 charged precursor ions were selected within an 4 m/z isolation window, fragmented by higher-energy collisional dissociation (HCD) in the HCD cell of the instrument and MS/MS spectra recorded within the orbitrap analyzer over an available scan range of 200 to 2,000 m/z at a resolution of 17,500 (at 400 m/z) in profile mode. The target value for automatic gain control was 100000 and the maximum ion time 50 ms; already fragmented ions were excluded from further fragmentation for 10 seconds. Mass spectra were further processed within the Proteome Discoverer framework (version 1.4.1.14, Thermo Fisher Scientific) with standard parameters for spectrum selection. Searches were carried out in a modified version (in entries O70325 and Q91XR9 U converted into C) of the mouse SwissProt database (downloaded on 21th October 2015 from UniProt KB, containing 15660 entries) using the embedded Mascot search engine (version 2.4.1,

Matrix Science) with following parameters: tryptic cleavage specificity, maximal one missed cleavage site, 10 ppm precursor mass tolerance, 10 mmu fragment mass tolerance. Methionine oxidation and following modifications at cysteines were considered as variable modifications: dioxidation, trioxidation, glutathione, N-Ethylmaleimide (NEM) and carbamidomethyl. Identifications were accepted at a false discovery rate of 1% using the 'fixed value PSM validator' node. Precursor ion quantification of modified variants of the peptide GFVCIVTNVASQCGK was subsequently carried out in Skyline (version 3.5.0.9.3.1.9, MacCoss Lab, University of Washington, USA) and resulting peak areas from doubly and triply charged precursor ions normalized to the sum of the signals from the three unmodified GPX4 peptides TDVNYTQLVDLHAR, EFAAGYNVK and FLIDK.

Isolation of Mitochondria from MEFs

Isolation of mitochondria from MEFs was conducted using the pump-controlled cell rupture system (PCC) as previously described (Schmitt et al., 2013). In brief, 20-25 x 10⁶ MEFs per cell line were trypsinized and collected by centrifugation. The cell pellet was resuspended in isolation buffer (300 mM sucrose, 5 mM TES and 200 μM ethylene glycol-bis(2-aminoethylether)-*N,N,N',N'*-tetraacetic acid (EGTA), pH 7.2) given a cell density of ~5 x 10⁶ cells/ml. The cell suspension was then passed through the cell homogenizer with a clearance of 6 μm and 7 strokes at a speed rate of 700 μl/min. Cell debris and organelles were cleared from the homogenate by centrifugation at 800 x g for 5 min at 4°C. Mitochondria were collected at 9,000 x g (10 min, 4°C) and resuspended in fresh isolation buffer. Mitochondrial protein concentration was determined using the Bradford assay. For purification, mitochondria were loaded on a 24%/12% Nycodenz[®] gradient (Axis Shield) and centrifuged

at 30,000 × g for 15 min at 4°C in an ultracentrifuge (Beckman). Next, mitochondria were collected from the 12%/24% interphase, washed with isolation buffer and collected at 9,000 × g (10 min, 4°C). Isolated and purified mitochondria were either further used for functional assays or for immunoblot analysis using antibodies against mitochondrial proteins including citrate synthase (1:1000, Novus Biologicals), complex I-V (1:1000, Thermo Fisher Scientific).

Quantification of Mitochondria by Flow Cytometry

To compare the number of mitochondria isolated from different cell lines, 10N-nonyl acridine orange (NAO)-stained mitochondria were analyzed by flow cytometry together with two internal standards allowing the exact determination of the number of mitochondria (Schmitt et al., 2014). In brief, a diluted mitochondria suspension of 0.1 µg/ml was stained with 10 nM NAO (Invitrogen). A defined number of TruCOUNT™ beads (BD Biosciences) were mixed with 500 µl stained mitochondria and 20 µl of premixed Fluoresbrite® microspheres (diameter 0.94 µm, Polysciences Europe GmbH). Two measurements were performed assessing first the concentration of Fluoresbrite® microspheres in a defined volume by the determined number of TruCOUNT™ beads in that volume. The second measurement calculated the number of stained mitochondria by the number of determined Fluoresbrite® microspheres. Data was analyzed using the FlowJo software.

Mitochondrial Integrity Measurements

Mitochondrial integrity was assessed by measuring mitochondrial membrane potential ($\Delta\Psi_m$) using Rhodamine 123 (Rh123) (Invitrogen) and following the quenching of the

fluorescence signal every 90 sec over a period of 1 h (Schulz et al., 2013). To this end, mitochondria (final concentration 50 µg) were diluted in swelling assay buffer (0.2 M sucrose, 10 mM MOPS-Tris, 5 mM succinate, 1 mM Pi [H₃PO₄], 10 µM EGTA) and mixed with 500 nM Rh123 or additionally with 500 nM FCCP as negative control. Fluorescence was measured at 485/20 nm, 528/20 nm using the plate reader Fluorimeter Synergy (Biotek). For the swelling assay, the change of mitochondrial absorbance at 540 nm (Fluorimeter Synergy, Biotek) was monitored over a period of 1 h with additional treatment of the organelles with 100 µM CaCl₂ as negative control (Schulz et al., 2013).

Measurement of Mitochondrial H₂O₂ Release

Measurement of mitochondrial H₂O₂ release was determined according to Muller et al. (Muller et al., 2008). For the measurement of H₂O₂ release, 50 µg mitochondria were diluted in H₂O₂ assay buffer (KCl 125 mM, HEPES 10 mM, MgCl₂ 5 mM, K₂HPO₄ 2 mM, MnCl₂ 5 µM) and mixed with an inductor (glutamate/malate [G/M, 50 mM, respectively final concentration 12.5 mM], G/M and ADP [12.8 mM, final concentration 3.2 mM], G/M and rotenone [20 µM, final concentration 5 µM]) and an enzyme mix consisting of Amplex[®] Red (320 µM, final concentration 80 µM), superoxide dismutase (SOD, 60 U/ml, final 3 U) and horseradish peroxidase (HRP) (2 U/ml, final 0.5 U). Generation of H₂O₂ was assessed by measuring the fluorescence change of Amplex[®] Red (excitation: 540/20 nm; emission: 620/40 nm) every 90 sec over a period of 1 h using the plate reader Fluorimeter Synergy (Biotek). The generation of pmol H₂O₂ per min/mg protein was calculated by using a standard curve with defined H₂O₂ concentrations.

Measurement of ATP Production

ATP production of mitochondria was measured using glutamate (12.5 mM) / malate (12.5 mM) as substrates in a bioluminescence based assay using ATP Bioluminescence Assay Kit CLS II (Roche). 10 µg of mitochondrial suspension was used to perform the assay according to the manufacturer`s instructions.

Determination of Oxygen Consumption Rates (OCR)

20,000 cells/well were seeded on a 96-well plate (Seahorse) and incubated overnight in Standard DMEM. The medium of the cells was changed 1 h before the measurement to XFDMEM (Seahorse), supplemented with 25 mM glucose and 1 mM pyruvate. Oxygen consumption of MEFs was measured by the XFAnalyzer96 (Seahorse) over 3 hours at basal conditions, after injections of oligomycin (1 µg/ml), FCCP (1 µM) and antimycin A (2 µM) and rotenone (5 µM). Data was analyzed and oxygen consumption rate was assessed using the Seahorse Bioscience Wave program.

Cross-Breeding of Animals

Gpx4^{wt/cys} and *Gpx4*^{wt/ser} mice (the latter described in (Ingold et al., 2015)) were first cross-bred with Flpe recombinase expressing transgenic *Rosa26_Flpe* animals (Rodriguez et al., 2000) to delete the frt-flanked *neomycin phosphotransferase (neo)* gene of the transgenic *Gpx4* allele. *Gpx4*^{wt/cys} and *Gpx4*^{wt/ser} animals that were positive for the deletion of the *neo* gene and negative for the *Flpe* allele were further mated with *C57BL/6J* animals. These were then finally cross-bred with TAM inducible *Gpx4*^{flox/flox,Rosa26CreERT2} mice (Friedmann Angeli et al., 2014), yielding *Gpx4*^{cys/flox,Rosa26CreERT2} and *Gpx4*^{ser/flox,Rosa26CreERT2} mice among the control

mice. To obtain inducible disruption of the loxP-flanked *Gpx4* allele, mice (>8 weeks of age; males and females) were injected twice with 0.5 mg TAM dissolved in Mygliol.

QUANTIFICATION AND STATISTICAL ANALYSES

Statistics

Data in figure legends are presented as mean \pm s.d. or \pm s.e.m. values. The exact value of sample size (n) is given in the figure legends and indicates either the number of animals and tissues for in vivo experiments or number of cell clones in in vitro experiments or the number of experimental replicates. As a general rule for cell viability experiments, graphs show the mean \pm s.d. of n = 3 wells representative of a single experiment performed independently x times (x value is given in figure legends) for reproducibility. Statistical analyses were performed with GraphPad Prism 6.0 software using either unpaired two-tailed t test or one-way ANOVA for multiple comparison or Mantel-Cox test for survival analyses. Statistical significance was assessed at * $P < 0.05$, ** $P < 0.01$, *** $P < 0.001$, **** $P < 0.001$.

SUPPLEMENTAL ITEM TITELS

Supplementary Video 1. *Gpx4^{cys/cys}* Animals Suffer from Severe Epileptic Seizures, Related to Figure 1

Supplementary movie shows *Gpx4^{cys/cys}* mice together with control littermates (on a mixed *129S6SvEvTac* × *C57BL/6J* genetic background). *Gpx4^{cys/cys}* mice suffered from severe spontaneous seizures at the age of 15 days when touched by the experimenter or littermates.

Figure S1. Homozygous *Gpx4^{cys/cys}* Animals on a *C57BL/6J* Background die During Embryogenesis, Related to Figure 1

(A) Overview pictures of brain tissues derived from homozygous *Gpx4^{cys/cys}* mice and *Gpx4^{wt/wt}* littermates at the age of 16 days after birth showing a marked decrease of parvalbumin-positive (PV+) interneurons and the presence of terminal deoxynucleotidyl transferase dUTP nick end labeling (TUNEL)-positive cells in the cortex of homozygous mutant mice but not in the wt animals (one representative staining out of 3 brain tissues of each genotype is shown, scale bar = 100 μm).

(B) Immunohistochemical staining against other calcium-binding GABAergic interneurons, such as calbindin and calretinin, did not show any differences in their expression in *Gpx4^{wt/wt}* and *Gpx4^{cys/cys}* brains 16 days after birth (scale bars = 100 μm, one representative staining out of 5 brain tissues per genotype is shown).

(C) Analysis of embryos isolated at different gestational days (from E9.5 – E12.5; on the *C57BL/6J* background) revealed severe developmental malformations of the brain, hemorrhages (arrows), pericardial edema (arrows), growth retardation and overall paleness (one representative picture per genotype and time is shown; scale bars are given in the figures).

(D) Histopathological staining of paraffin-embedded embryos showed malformations of the developing heart including pericardial edema and decreased trabeculation (scale bars = 100 μ M, one representative staining per genotype and time is displayed).

Figure S2. Adult Animals Expressing the Cys Variant of Gpx4 do not Show Any Signs of Kidney Damage, Related to Figure 2

(A,B) Measurement of creatinine (A) and blood urea nitrogen (B), both markers for kidney function, performed 40 days after TAM administration, were unaltered in *Gpx4^{flox/cys;Rosa26_CreERT2}* compared to control mice.

(C) Quantitative real-time PCR of markers for proximal tubule stress indicated by *kidney injury molecule -1 (Kim-1)*, *tissue inhibitor of metalloproteinase 2 (Timp-2)* and *insulin-like growth factor-binding protein 7 (Igfbp7)* were measured from kidney tissues isolated 40 days after TAM administration showed no difference between *Gpx4^{flox/cys;Rosa26_CreERT2}* and control animals (data presents the mean \pm s.d; n = 6 animals per genotype (A, B, and C)).

Figure S3. Peroxiredoxin-3 Expression is Slightly Increased in *Gpx4^{cys/cys}* MEFs, Related to Figure 3

Immunoblot analysis of various professional antioxidant proteins showed a slight increase in expression only for peroxiredoxin-3 (PRX3) in *Gpx4^{cys/cys}* cell clones, while no differences were detected for peroxiredoxins-1/-2 (PRX1, PRX2) and cytosolic (TXNRD1) and mitochondrial thioredoxin reductases (TXNRD2) (one representative experiment out of 2 is shown).

Figure S4. Peroxides and Complex I Inhibitors of the Mitochondrial Respiratory Chain Induce Cell Death in *Gpx4^{cys/cys}* Cells at Low Concentrations, Related to Figure 4

(A) Treatment with cholesterol hydroperoxide (ChOOH), a GPX4 substrate, efficiently induced cell death in *Gpx4^{cys/cys}* cells at very low concentrations compared to control cells.

(B) *Gpx4^{cys/cys}* cells showed increased sensitivity towards complex I inhibitors, rotenone and phenformin.

(C) *Gpx4^{wt/wt}* and *Gpx4^{cys/cys}* MEFs were equally resistant to different cytotoxic compounds, such as cyanide-p-trifluoromethoxyphenylhydrazine (FCCP), menadione, mitoxantrone, nocodazol, irinotecan, vinoblastine, PAO and sulforaphane. *Gpx4^{cys/cys}* MEFs were more sensitive towards treatments with complex III inhibitors, antimycin A and myxothiazol, while dosage effects were not observed.

(D) *Gpx4^{cys/cys}* MEFs were more resistant towards the established ferroptosis inducers (1*S*,3*R*)-RSL3 (a GPX4 inhibitor), and the glutathione depriving agents erastin and L-buthionine sulfoximine (BSO).

(E) Measurement of total intracellular glutathione detected higher glutathione levels in mutant cells (n = 3 replicates of one representative experiment, statistics was assessed using two-tailed t test **P*<0.05)

(F) PFa1 cells (Seiler et al., 2008) expressing doxycycline (Dox) dependent exogenous wildtype and GPX4-Cys were treated with different doxycycline concentrations. To achieve equal expression of wt GPX4 and GPX4-Cys (U46C), cells were supplemented with either 10 µg/ml (wt) or 1 µg/ml Dox (U46C) followed by (1S,3R)-RSL3 treatment. PFa1 cells expressing the Cys variant demonstrated a much higher resistance towards RSL3 than wt GPX4 expressing cells (data represents the mean ± s.d. of n = 3 wells from 1 representative experiment performed independently 2 (A) or 3 times (B, C, D, F)).

Figure S5. Homozygous *Gpx4*^{cys/cys} Cells Generate more ATP than Wildtype Cells

(A) Transmission electron microscopy (TEM) analysis of whole cells revealed differences in mitochondrial morphology between *Gpx4*^{wt/wt} and *Gpx4*^{cys/cys} under basal and peroxide treated conditions. Under H₂O₂ (100 µM) and rotenone (1 µM) treated conditions *Gpx4*^{cys/cys} mitochondria showed outer membrane rupture and shrinkage of cristae. The same structural alterations were observed in *Gpx4*^{wt/wt} cells treated with the GPX4 inhibitor (1S,3R)-RSL3 (10 nM) as reportedly previously (Doll et al., 2017; Friedmann Angeli et al., 2014) (scale bars 1600 x = 2 µM; 10000 x = 500 nm).

(B) Isolated mitochondria derived from both *Gpx4*^{wt/wt} and *Gpx4*^{cys/cys} cells presented the same stable mitochondrial membrane potential ($\Delta\Psi_m$).

(C) As determined by Amplex[®] Red, H₂O₂ release of isolated *Gpx4*^{wt/wt} and *Gpx4*^{cys/cys} mitochondria did not show any differences.

(D-E) Mitochondria of *Gpx4*^{cys/cys} cells differed in size compared to mitochondria of *Gpx4*^{wt/wt} cells. They appeared with lower optical density (D) and tended to have lower protein content per 10¹⁰ mitochondria (E).

(F) Mitochondrial (mt) RNA was found to be increased in *Gpx4^{cys/cys}* mitochondria.

(G) Immunoblot analysis of mitochondrial respiratory chain complexes revealed an increased expression of Complex IV in *Gpx4^{cys/cys}* mitochondria (shown is one representative experiment performed independently 4 times).

(H) Determination of the oxygen consumption rate (OCR) on whole cells using XF Seahorse demonstrated an increased basal respiration rate (1) and ATP-linked respiration (2) in *Gpx4^{cys/cys}* cells. Data present mean \pm s.e.m. of n = 4 wells from 1 representative experiment performed independently 4 times.

(I) ATP generation measurement on isolated mitochondria confirmed that *Gpx4^{cys/cys}* cells produce ~3 times more ATP than wt cells (data represent the mean \pm s.d. of n = 5 (B, D, I); n = 4 (C) n = 3 (E, F). Statistical analysis was conducted using two-tailed t-test * $P < 0.5$, *** $P < 0.001$).

Figure S6. Peroxides Induce Ferroptotic Cell Death in *Gpx4^{cys/cys}* but not Wildtype Cells, Related to Figure 4

(A-C) Cell death induced by ChOOH (A), tBOOH (B) and rotenone (C) could be prevented by ferroptosis inhibitors only in homozygous *Gpx4^{cys/cys}* but not in *Gpx4^{wt/wt}* MEFs. Data present the mean \pm s.d. of n = 3 wells from 1 representative experiment performed independently 3 times.

(D) Treatment with polyunsaturated fatty acids (PUFA) induced cell death at very low concentrations in homozygous *Gpx4^{cys/cys}* but not in *Gpx4^{wt/wt}* MEFs. Data present the mean \pm s.d. of n = 3 wells from 1 representative experiment performed independently 2 times.

Figure S7. GPX4 Protein Sequence Alignment of Different Organisms, Related to Figure 6

GPX4 sequence alignment of *Homo sapiens* (*H. sapiens*, P36969), *Mus musculus* (*M. musculus*, O70325), *Seriola lalandi* (*S. lalandi*, F8UV59), *Gallus gallus* (*G. gallus*, Q8QG67), *Canarypox virus* (*C. virus*, Q6VZR0), *Trypanosoma brucei brucei* (*T. brucei brucei*, D6XK30), *Arabidopsis thaliana* (*A. thaliana*, Q8L910), *Caenorhabditis elegans* (*C. elegans*, Q9N2X2).

The active site, which is marked in red with an asterisk, consistently contains Sec in higher vertebrates. The amino acids Gln, Trp and Asn that are part of the catalytic tetrad are marked in blue and are highly conserved across all the listed organisms.

KEY RESOURCES TABLE

The table highlights the genetically modified organisms and strains, cell lines, reagents, software, and source data **essential** to reproduce results presented in the manuscript. Depending on the nature of the study, this may include standard laboratory materials (i.e., food chow for metabolism studies), but the Table is **not** meant to be comprehensive list of all materials and resources used (e.g., essential chemicals such as SDS, sucrose, or standard culture media don't need to be listed in the Table). **Items in the Table must also be reported in the Method Details section within the context of their use.** The number of **primers and RNA sequences** that may be listed in the Table is restricted to no more than ten each. If there are more than ten primers or RNA sequences to report, please provide this information as a supplementary document and reference this file (e.g., See Table S1 for XX) in the Key Resources Table.

Please note that ALL references cited in the Key Resources Table must be included in the References list. Please report the information as follows:

- **REAGENT or RESOURCE:** Provide full descriptive name of the item so that it can be identified and linked with its description in the manuscript (e.g., provide version number for software, host source for antibody, strain name). In the Experimental Models section, please include all models used in the paper and describe each line/strain as: model organism: name used for strain/line in paper: genotype. (i.e., Mouse: OXTR^{fl/fl}; B6.129(SJL)-Oxtr^{tm1.1Wsy/J}). In the Biological Samples section, please list all samples obtained from commercial sources or biological repositories. Please note that software mentioned in the Methods Details or Data and Software Availability section needs to be also included in the table. See the sample Table at the end of this document for examples of how to report reagents.
- **SOURCE:** Report the company, manufacturer, or individual that provided the item or where the item can be obtained (e.g., stock center or repository). For materials distributed by Addgene, please cite the article describing the plasmid and include "Addgene" as part of the identifier. If an item is from another lab, please include the name of the principal investigator and a citation if it has been previously published. If the material is being reported for the first time in the current paper, please indicate as "this paper." For software, please provide the company name if it is commercially available or cite the paper in which it has been initially described.
- **IDENTIFIER:** Include catalog numbers (entered in the column as "Cat#" followed by the number, e.g., Cat#3879S). Where available, please include unique entities such as [RRIDs](#), Model Organism Database numbers, accession numbers, and PDB or CAS IDs. For antibodies, if applicable and available, please also include the lot number or clone identity. For software or data resources, please include the URL where the resource can be downloaded. Please ensure accuracy of the identifiers, as they are essential for generation of hyperlinks to external sources when available. Please see the Elsevier [list of Data Repositories](#) with automated bidirectional linking for details. When listing more than one identifier for the same item, use semicolons to separate them (e.g. Cat#3879S; RRID: AB_2255011). If an identifier is not available, please enter "N/A" in the column.
 - **A NOTE ABOUT RRIDs:** We highly recommend using RRIDs as the identifier (in particular for antibodies and organisms, but also for software tools and databases). For more details on how to obtain or generate an RRID for existing or newly generated resources, please [visit the RII](#) or [search for RRIDs](#).

Please use the empty table that follows to organize the information in the sections defined by the subheading, skipping sections not relevant to your study. Please do not add subheadings. To add a row, place the cursor at the end of the row above where you would like to add the row, just outside the right border of the table. Then press the ENTER key to add the row. You do not need to delete empty rows. Each entry must be on a separate row; do not list multiple items in a single table cell. Please see the sample table at the end of this document for examples of how reagents should be cited.

TABLE FOR AUTHOR TO COMPLETE

Please upload the completed table as a separate document. **Please do not add subheadings to the Key Resources Table.** If you wish to make an entry that does not fall into one of the subheadings below, please contact your handling editor. (NOTE: For authors publishing in Current Biology, please note that references within the KRT should be in numbered style, rather than Harvard.)

KEY RESOURCES TABLE

REAGENT or RESOURCE	SOURCE	IDENTIFIER
Antibodies		
Anti-GPX4, rabbit monoclonal	Abcam	Cat#125066, RRID:AB_10973901
Anti-Dimedone, rabbit polyclonal	This paper	N/A
Anti-HA-tag, rat monoclonal, Clone 3F10	Roche	Cat#12158167001, RRID:AB_390915
Anti-ACSL4, mouse monoclonal	Santa Cruz	Cat#Sc-271800, RRID:AB_10715092
Anti-TXNRD1, rat monoclonal	Telorack et al. 2015	N/A
Anti-TXNRD2, rat monoclonal, Clone 1C4	Mandal et al.	N/A
Anti-GPX1, rabbit polyclonal	Abcam	Cat#Ab22604, RRID:AB_2112120
Anti- β -actin, mouse monoclonal	Sigma	Cat#A5441, RRID:AB_476744
Anti-Parvalbumin, mouse monoclonal	Swant	Cat# PV235
Anti-GFAP, rabbit monoclonal	Cell signaling	Cat#12389, RRID:AB_2631098
Anti-IBA1, rabbit polyclonal	Genetex	Cat# GTX10042
Anti-Calbindin, rabbit antiserum	Swant	Cat#CB-38a
Anti-Calretinin, rabbit polyclonal	Swant	Cat#CR7697, RRID:AB_2619710
Anti-active Caspase 3, rabbit polyclonal	Cell signaling	Cat#9661, RRID:AB_2341188
Anti-Citrate synthase, rabbit polyclonal	Novus Biologicals	Cat#NBP2-13878
Anti-Complex I-V, mouse monoclonal	Thermo Fisher Scientific	Cat#458099, RRID:AB_2533835
Anti-Peroxiredoxin 1, rabbit polyclonal	Godoy et al. 2011	N/A
Anti-Peroxiredoxin 2, rabbit polyclonal	Lillig Lab	N/A
Anti-Peroxiredoxin 3, rabbit polyclonal	Godoy et al. 2011	N/A
Biotinylated goat anti-rabbit IgG	Vector Laboratories	Cat#BA-1000, RRID:AB_2313606
Biotinylated goat anti-mouse IgG (H+L)	Vector Laboratories	Cat#BA-9200, RRID:AB_2336171
Goat anti-rabbit IgG-HRP, polyclonal	Santa Cruz	Cat#SC-2030, RRID:AB_631747
Goat anti-mouse IgG-HRP, polyclonal	Santa Cruz	Cat# SC-2031, RRID:AB_631737
Goat anti-rat IgG-HRP (H+L), polyclonal	Jackson ImmunoResearch	Cat#112-035-062 RRID:AB_2338133
IRDye 800CW goat anti-rabbit IgG (H+L)	LI-COR	Cat#925-32210, RRID:AB_2687825
IRDye 680RD goat anti-rat (IgG (H+L)	LI-COR	Cat#925-68076
Donkey anti-goat IgG (H+L) Alexa Fluor 594, cross-adsorbed polyclonal	Thermo Fisher Scientific	Cat#A11058, RRID:AB_2534105

Donkey anti-rabbit IgG (H+L) Alexa Fluor 488, cross-adsorbed polyclonal	Thermo Fisher Scientific	Cat#A21206 RRID:AB_2535792
Bacterial and Virus Strains		
<i>DH5α E.coli</i>	Thermo Fisher Scientific	Cat#18265017
Biological Samples		
Chemicals, Peptides, and Recombinant Proteins		
X-tremeGene HP DNA transfection	Sigma-Aldrich	Cat#06366236001
AquaBluer® Cell Viability Assay Solution	Multi Target Pharmaceuticals	Cat#6015
4-Hydroxy-Tamoxifen	Sigma-Aldrich	Cat#H7954
Doxycycline hyclate	Sigma-Aldrich	Cat#D9891
(1S,3R)-RSL3	Dixon et al. 2012	N/A
BODIPY 581/591 C11	Invitrogen	Cat#D3861
α-Tocopherol	Sigma-Aldrich	Cat#T3251
Z-VAD-FMK	Enzo Life Science	Cat#Alx-260-020-M001
Necrostatin-1	Sigma	Cat#N9037
Necrostatin-1S	BioVision	Cat#2263
Ciclopirox olamine	Sigma	Cat#C2162700
Erastin	Sigma-Aldrich	Cat#E7781
L-Buthionine-sulfoximine (BSO)	Sigma-Aldrich	Cat#B2515
Ferrostatin-1	Xcessbio Biosciences	Cat#M60042-2S
Liproxstatin-1	Sigma	Cat#SML-1414
XF Assay Medium Modified DMEM	Seahorse Bioscience	Cat#102365-100
Tert-butyl hydroperoxide (tBOOH)	Sigma-Aldrich	Cat#458139
Cholesterol hydroperoxide (ChOOH)	This paper	N/A
Antimycin A	Sigma-Aldrich	Cat#A8674
Auranofin	Sigma-Aldrich	Cat#A6733
Rotenone	Sigma-Aldrich	Cat#R8875
Phenformin hydrochloride	Sigma-Aldrich	Cat#P7045
Myxothiazol	Sigma-Aldrich	Cat#T5580
10N-nonyl acridine orange (NAO)	Invitrogen	Cat#A-1372
TruCOUNT™ beads	BD Biosciences	Cat#340334
Fluoresbrite® YG Microspheres 0.94 μm	Polysciences Europe	N/A
Rhodamine 123	Invitrogen	Cat#R302
Na ₂ ⁷⁵ SeO ₃	POLATOM	Cat#RSe-2
Methyl-PEG-Maleimide Reagent (mm(Peg)24)	Thermo Fisher Scientific	Cat#22713
Amplex Red	Life technologies	Cat#A12222

Critical Commercial Assays		
Gibson Assembly® Master Mix	New England Biolabs	Cat#E2511
ApopTag Fluorescein In Situ Apoptosis Detection Kit	Merck-Millipore	Cat#S7110
ApopTag Peroxidase In Situ Apoptosis Detection Kit	Merck-Millipore	Cat#S7100
QIAGEN® PCR cloning Kit	Qiagen	Cat# 231124
Vectastain ABC Kit	Vector Laboratories	Cat#PK-6100
Vectastain DAB Kit	Vector Laboratories	Cat#SK-4100
Creatinine FS Set	DiaSys	Cat#117119910026
Urea FS Kit	DiaSys	Cat#131019910920
ATP Bioluminescence Assay Kit CLS II	Roche	Cat#11699695001
Deposited Data		
Experimental Models: Cell Lines		
Mouse: murine embryonic fibroblasts	This paper	N/A
Mouse: PFA1 cells	Seiler et al. 2008	N/A
Mouse: FSH-tagged wildtype GPX4	This paper	N/A
Mouse: FSH-tagged Cys GPX4	This paper	N/A
Mouse: doxycycline-dependent FHS-tagged wildtype GPX4	This paper	N/A
Mouse: doxycycline-dependent FHS-tagged Cys GPX4	This paper	N/A
Mouse: FSH-tagged allCys/Ser Cys GPX4	Mannes et al. 2011	N/A
Mouse: IDG3.2-rosa26	Hitz et al. 2007	N/A
Human: HEK293T	Clontech	Cat#632180
Experimental Models: Organisms/Strains		
Mouse:Rosa26_Flpe:WT	Rodriguez et al. 2000	N/A
Mouse:Gpx4 ^{fl/fl} ;Rosa26_CreERT2	Angeli et al. 2014	N/A
Mouse:Gpx4 ^{fl/fl} ;Rosa26_CreERT2;Gpx4 ^{fl/ser} ;Rosa26_CreERT2	This Paper	N/A
Mouse:Gpx4 ^{fl/fl} ;Rosa26_CreERT2;Gpx4 ^{fl/cys} ;Rosa_CreERT2	This Paper	N/A
Mouse:Gpx4 ^{fl/fl} ;Rosa26_CreERT2;Gpx4 ^{fl/wt} ;Rosa_CreERT2	This Paper	N/A
Mouse:C57BL6/J.Sv129Ev:Gpx4 ^{wt/cys}	This Paper	N/A
Mouse:C57BL6/J:Gpx4 ^{wt/cys}	This Paper	N/A
Mouse:C57BL6/J:Gpx4 ^{wt/ser}	Ingold et al. 2015	N/A
Oligonucleotides		
CRISPR sgRNA AcsI4	Doll et al. 2017	N/A
TaqMan® Gpx4 FAM	Applied Biosystems	Cat#4331182
TaqMan® Hprt VIC	Applied Biosystems	Cat#4448489
TaqMan® MT-RNRN1 FAM	Applied Biosystems	Cat#4331182
CRISPR sgRNA Trsp (fwd) 5'-CACCGCTCTGTGCTAAACAGCTACGT-3'	This paper (Invitrogen)	N/A

CRISPR sgRNA Trsp (rev) 5'-TAAAACGTAGCTGTTTAGCGACAGAGC-3'	This paper (Invitrogen)	N/A
PCR primers see Table S2	This paper (Invitrogen)	N/A
Recombinant DNA		
Plasmid: pPNT4.1	Seiler et al. 2008	N/A
Plasmid: pPNT4.8	Seiler et al. 2008	N/A
Plasmid: pPAF-1	This paper	N/A
Plasmid: 442-PL1-IRES-puro	Seiler et al. 2008	N/A
Plasmid: pEcoEnv-IRES-puro	Seiler et al. 2008	N/A
Plasmid: pMDLg_pRRE	Seiler et al. 2008	N/A
Plasmid: pRSV_Rev	Seiler et al. 2008	N/A
Plasmid: 442-puro-FSH-tagged wildtype GPX4	Mannes et al. 2011	N/A
Plasmid: 442-puro-FSH-tagged Cys-GPX4	This paper	N/A
Plasmid: 442-puro-FSH-tagged allCys/Ser Cys-GPX4	Mannes et al. 2011	N/A
Plasmid: pKLV-U6gRNA(Bbs1)-PGKpuro2ABFP	Koike-Yusa et al. 2014	Addgene Cat#50946
Plasmid: pLentiCas9-Blast	Sanjana et al. 2014	Addgene Cat#52962
Plasmid: pRTS1	Bornkamm et al. 2005	N/A
Plasmid: pRTS1-FSH-tagged wildtype GPX4	Mannes et al. 2011	N/A
Plasmid: pRTS1-FSH-tagged Cys-GPX4	This paper	N/A
FSH-tagged Cys GPX4	Invitrogen	N/A
Software and Algorithms		
GraphPad Prism 6.0	GraphPad Software Inc.	www.graphpad.com
FlowJo V10	FlowJo LLC	https://www.flowjo.com/solutions/flowjo/downloads
ImageJ	NIH	https://imagej.nih.gov/ij/download.html
TIDE: Tracking of Indels by DEcomposition	Brinkmann et al. 2014	www.tide.nki.nl
Wave XFe Analyzer 2.2.0	Seahorse Bioscience	http://www.agilent.com/en-us/products/cell-analysis-(seahorse)/software-download-for-wave-desktop
Chromeleon 6.80 SR13	Thermo Fisher Scientific	CHROMELEON6
Xcalibur 4.0	Thermo Fisher Scientific	OPTON-30487
Skyline version 3.5.0.9.3.1.9	Thermo Fisher Scientific	https://skyline.ms
Proteome discoverer 1.4.1.14	Thermo Fisher Scientific	http://planetorbitrap.com/proteome-discoverer
CRISPRscan	Moreno-Mateos et al. 2015	http://www.crisprscan.org/
Other		

TABLE WITH EXAMPLES FOR AUTHOR REFERENCE

REAGENT or RESOURCE	SOURCE	IDENTIFIER
Antibodies		
Rabbit monoclonal anti-Snail	Cell Signaling Technology	Cat#3879S; RRID: AB_2255011
Mouse monoclonal anti-Tubulin (clone DM1A)	Sigma-Aldrich	Cat#T9026; RRID: AB_477593
Rabbit polyclonal anti-BMAL1	This paper	N/A
Bacterial and Virus Strains		
pAAV-hSyn-DIO-hM3D(Gq)-mCherry	Krashes et al., 2011	Addgene AAV5; 44361-AAV5
AAV5-EF1a-DIO-hChR2(H134R)-EYFP	Hope Center Viral Vectors Core	N/A
Cowpox virus Brighton Red	BEI Resources	NR-88
Zika-SMGC-1, GENBANK: KX266255	Isolated from patient (Wang et al., 2016)	N/A
<i>Staphylococcus aureus</i>	ATCC	ATCC 29213
<i>Streptococcus pyogenes</i> : M1 serotype strain: strain SF370; M1 GAS	ATCC	ATCC 700294
Biological Samples		
Healthy adult BA9 brain tissue	University of Maryland Brain & Tissue Bank; http://medschool.umaryland.edu/btbank/	Cat#UMB1455
Human hippocampal brain blocks	New York Brain Bank	http://nybb.hs.columbia.edu/
Patient-derived xenografts (PDX)	Children's Oncology Group Cell Culture and Xenograft Repository	http://cogcell.org/
Chemicals, Peptides, and Recombinant Proteins		
MK-2206 AKT inhibitor	Selleck Chemicals	S1078; CAS: 1032350-13-2

SB-505124	Sigma-Aldrich	S4696; CAS: 694433-59-5 (free base)
Picrotoxin	Sigma-Aldrich	P1675; CAS: 124-87-8
Human TGF- β	R&D	240-B; GenPept: P01137
Activated S6K1	Millipore	Cat#14-486
GST-BMAL1	Novus	Cat#H00000406-P01
Critical Commercial Assays		
EasyTag EXPRESS 35S Protein Labeling Kit	Perkin-Elmer	NEG772014MC
CaspaseGlo 3/7	Promega	G8090
TruSeq ChIP Sample Prep Kit	Illumina	IP-202-1012
Deposited Data		
Raw and analyzed data	This paper	GEO: GSE63473
B-RAF RBD (apo) structure	This paper	PDB: 5J17
Human reference genome NCBI build 37, GRCh37	Genome Reference Consortium	http://www.ncbi.nlm.nih.gov/projects/genome/assembly/grc/human/
Nanog STILT inference	This paper; Mendeley Data	http://dx.doi.org/10.17632/wx6s4mj7s8.2
Affinity-based mass spectrometry performed with 57 genes	This paper; and Mendeley Data	Table S8; http://dx.doi.org/10.17632/5hvpvspw82.1
Experimental Models: Cell Lines		
Hamster: CHO cells	ATCC	CRL-11268
<i>D. melanogaster</i> : Cell line S2: S2-DRSC	Laboratory of Norbert Perrimon	FlyBase: FBtc0000181
Human: Passage 40 H9 ES cells	MSKCC stem cell core facility	N/A
Human: HUES 8 hESC line (NIH approval number NIHhESC-09-0021)	HSCI iPS Core	hES Cell Line: HUES-8
Experimental Models: Organisms/Strains		
<i>C. elegans</i> : Strain BC4011: srl-1(s2500) II; dpy-18(e364) III; unc-46(e177)rol-3(s1040) V.	Caenorhabditis Genetics Center	WB Strain: BC4011; WormBase: WBVar00241916
<i>D. melanogaster</i> : RNAi of Sxl: y[1] sc[*] v[1]; P{TRiP.HMS00609}attP2	Bloomington Drosophila Stock Center	BDSC:34393; FlyBase: FBtp0064874
<i>S. cerevisiae</i> : Strain background: W303	ATCC	ATTC: 208353
Mouse: R6/2: B6CBA-Tg(HDexon1)62Gpb/3J	The Jackson Laboratory	JAX: 006494
Mouse: OXTRfl/fl: B6.129(SJL)-Oxtr ^{tm1.1Wsy/J}	The Jackson Laboratory	RRID: IMSR_JAX:008471
Zebrafish: Tg(Shha:GFP)t10: t10Tg	Neumann and Nuesslein-Volhard, 2000	ZFIN: ZDB-GENO-060207-1
<i>Arabidopsis</i> : 35S::PIF4-YFP, BZR1-CFP	Wang et al., 2012	N/A
<i>Arabidopsis</i> : JYB1021.2: pS24(AT5G58010)::cS24:GFP(-G):NOS #1	NASC	NASC ID: N70450

Oligonucleotides		
siRNA targeting sequence: PIP5K I alpha #1: ACACAGUACUCAGUUGAUA	This paper	N/A
Primers for XX, see Table SX	This paper	N/A
Primer: GFP/YFP/CFP Forward: GCACGACTTCTTCAAGTCCGCCATGCC	This paper	N/A
Morpholino: MO-pax2a GGTCTGCTTTGCAGTGAATATCCAT	Gene Tools	ZFIN: ZDB- MRPHLNO-061106- 5
ACTB (hs01060665_g1)	Life Technologies	Cat#4331182
RNA sequence: hnRNPA1_ligand: UAGGGACUUAGGGUUCUCUCUAGGGACUUAG GGUUCUCUCUAGGGA	This paper	N/A
Recombinant DNA		
pLVX-Tight-Puro (TetOn)	Clontech	Cat#632162
Plasmid: GFP-Nito	This paper	N/A
cDNA GH111110	Drosophila Genomics Resource Center	DGRC:5666; FlyBase:FBcl013041 5
AAV2/1-hsyn-GCaMP6- WPRE	Chen et al., 2013	N/A
Mouse raptor: pLKO mouse shRNA 1 raptor	Thoreen et al., 2009	Addgene Plasmid #21339
Software and Algorithms		
Bowtie2	Langmead and Salzberg, 2012	http://bowtie- bio.sourceforge.net/ bowtie2/index.shtml
Samtools	Li et al., 2009	http://samtools.sourc eforge.net/
Weighted Maximal Information Component Analysis v0.9	Rau et al., 2013	https://github.com/C hristophRau/wMICA
ICS algorithm	This paper; Mendeley Data	http://dx.doi.org/10.1 7632/5hvpvspw82.1
Other		
Sequence data, analyses, and resources related to the ultra-deep sequencing of the AML31 tumor, relapse, and matched normal.	This paper	http://aml31.genome .wustl.edu
Resource website for the AML31 publication	This paper	https://github.com/ch risamiller/aml31Supp Site

Figure 1

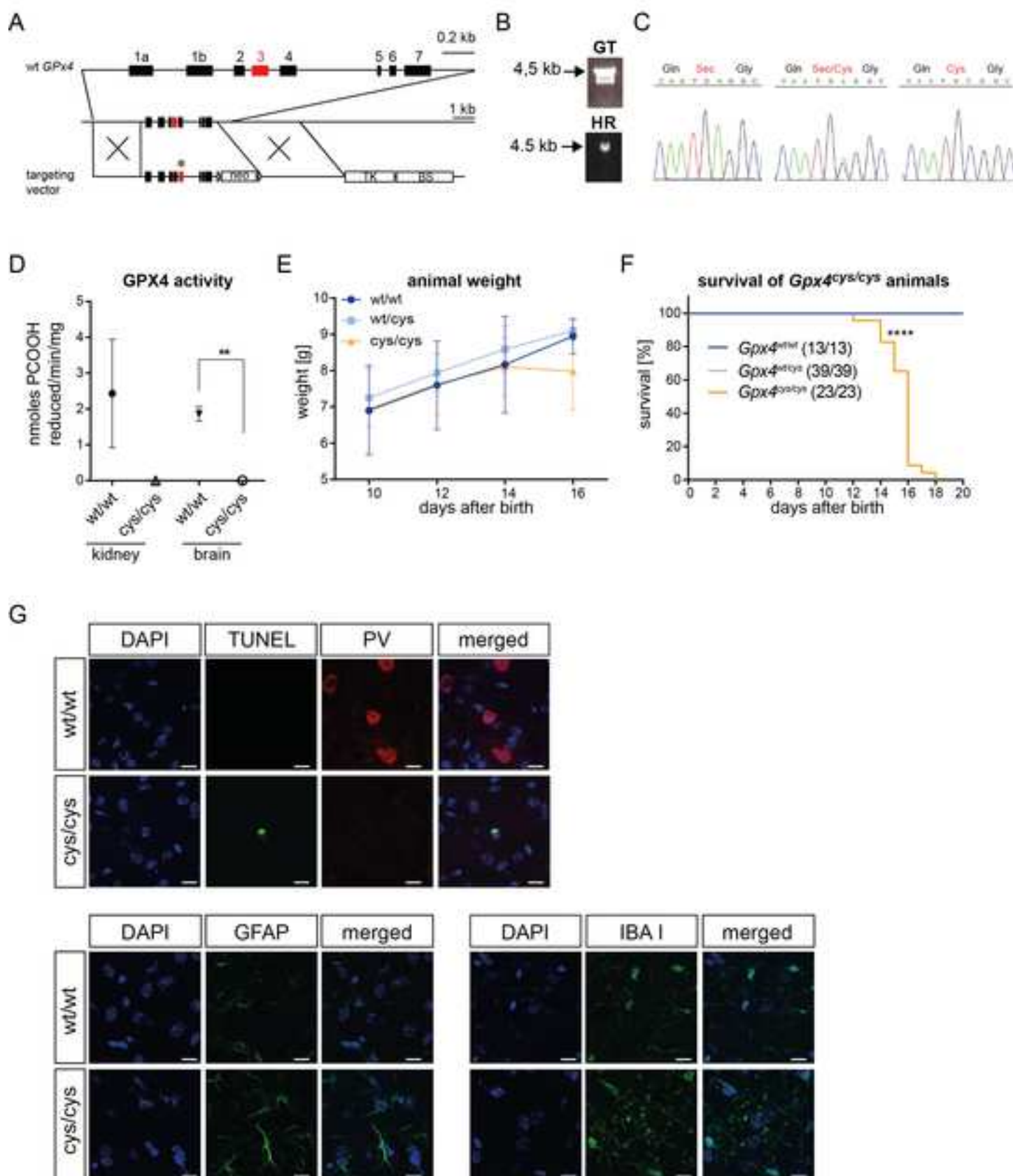


Figure 2

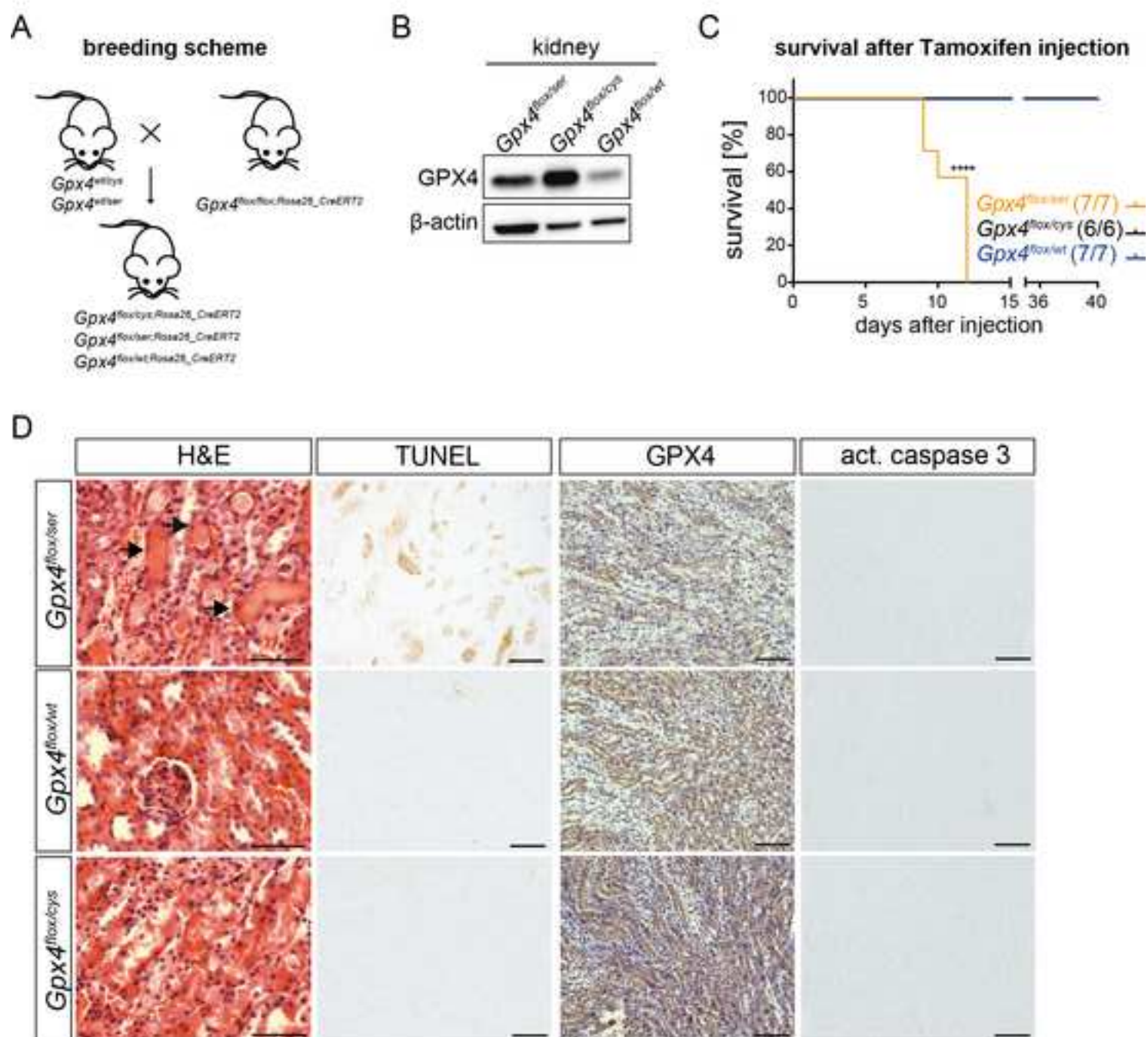


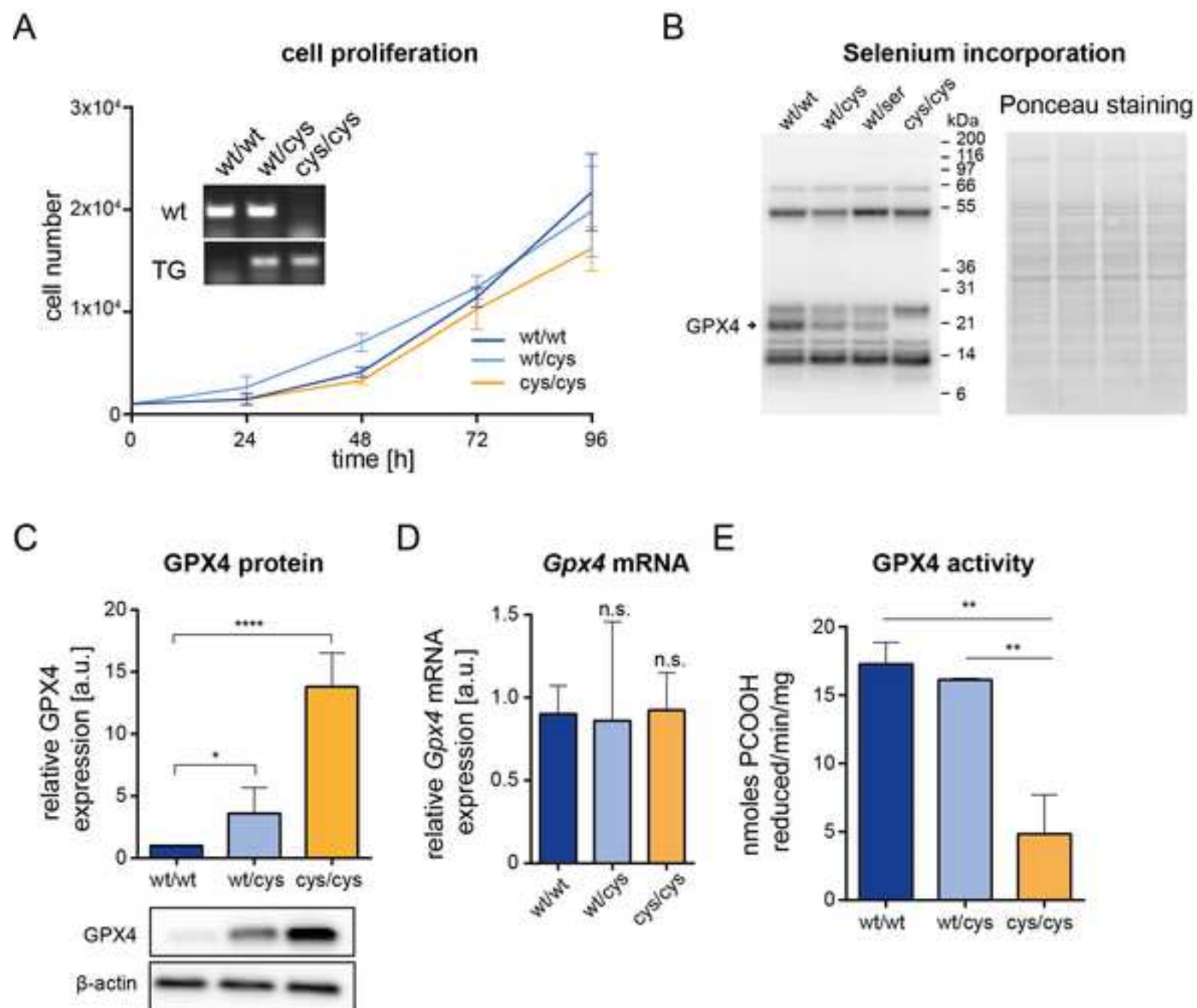
Figure 3

Figure 4

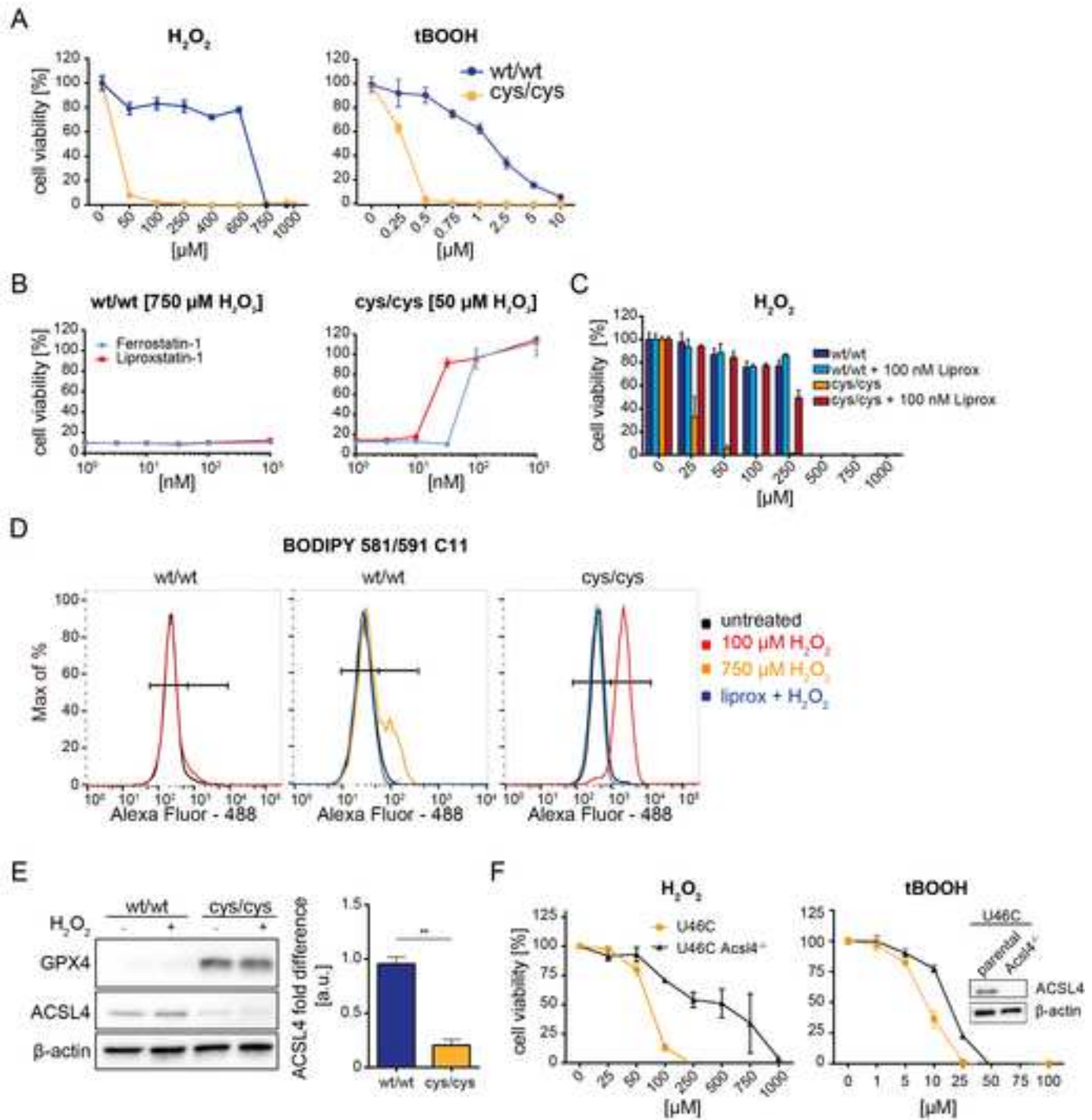


Figure 5

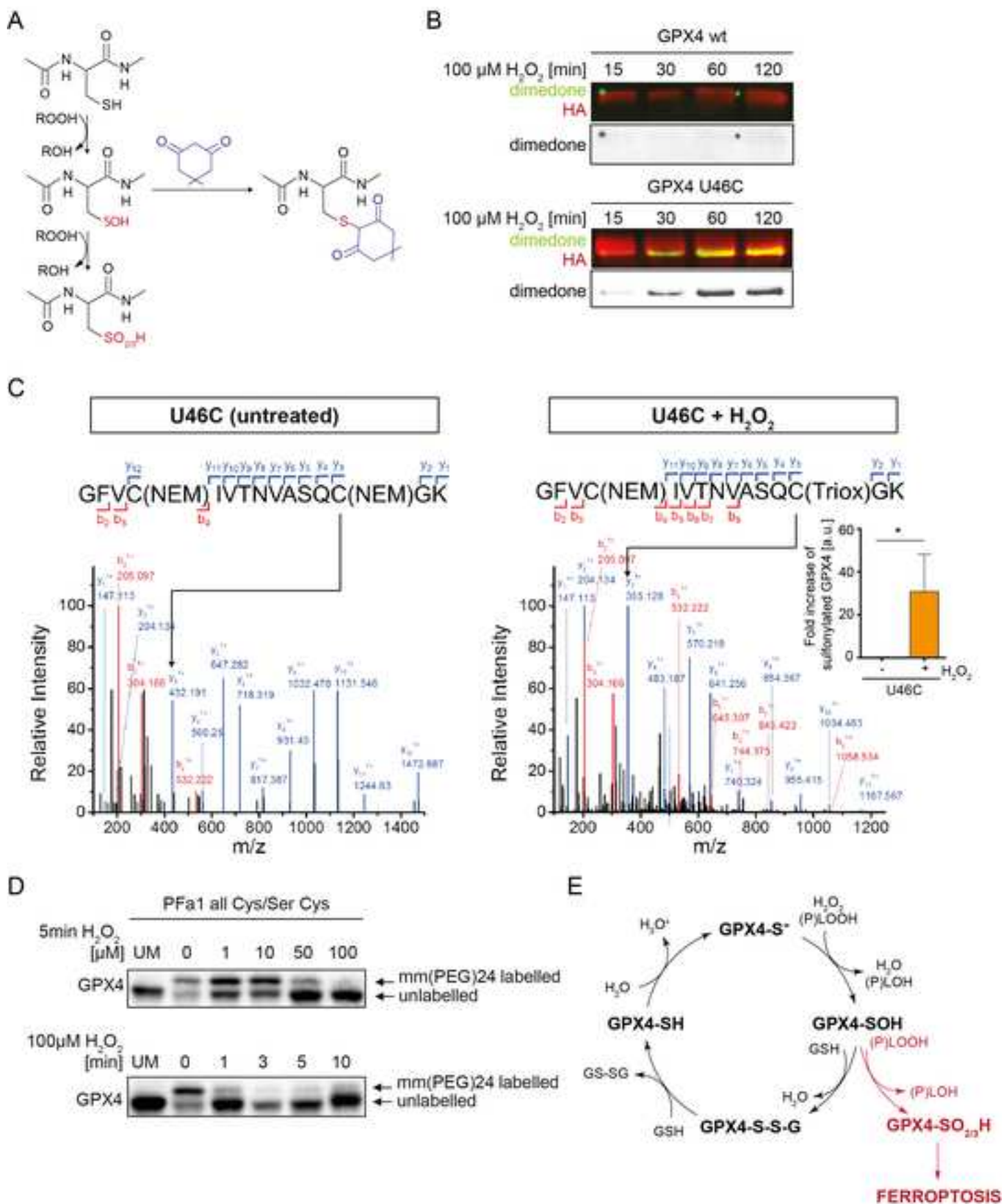


Figure 6

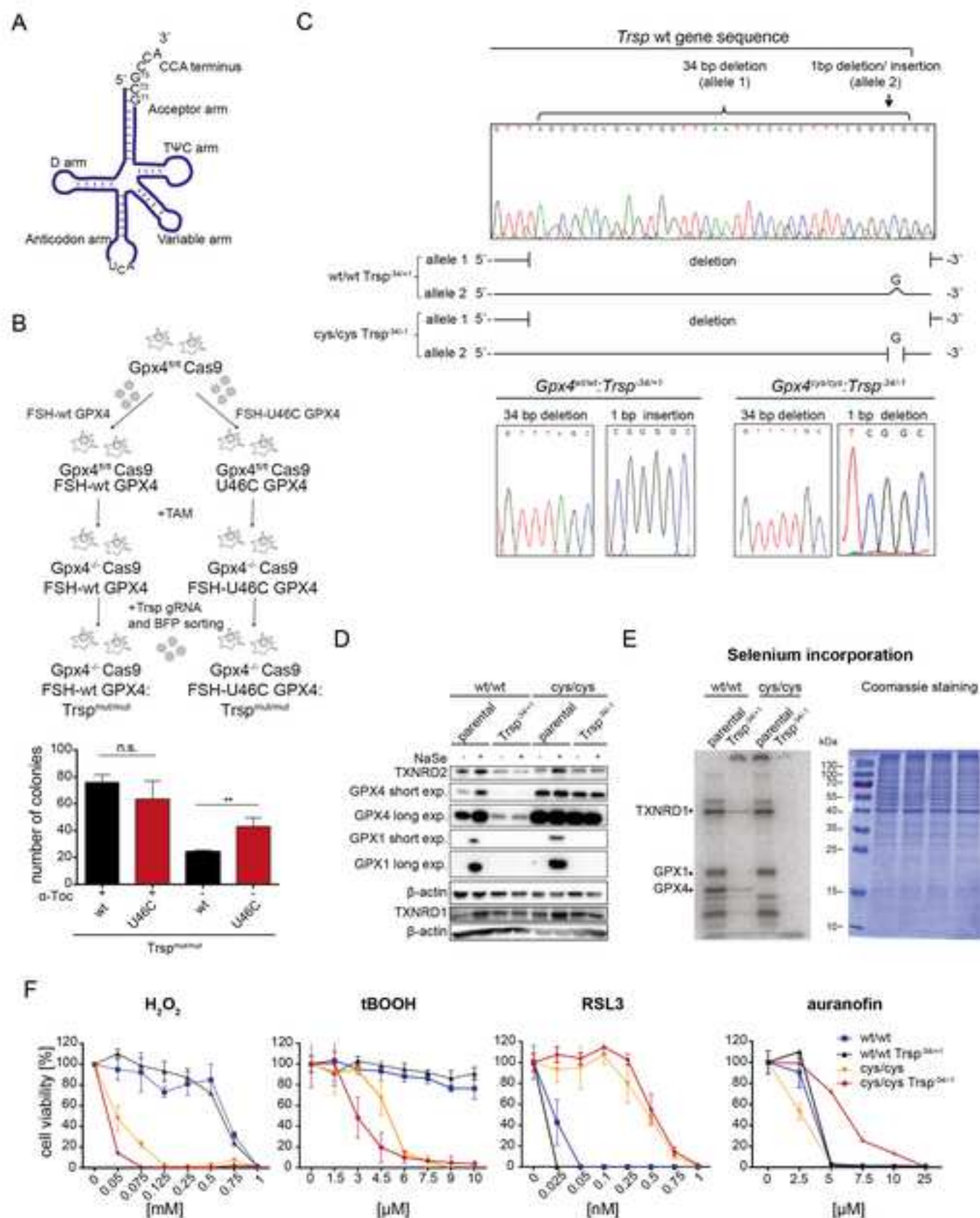


Table S1. Genotyping of Embryos at Different Gestational Days Obtained from Heterozygous *Gpx4*^{cys/wt} Breedings on a *C57BL/6J* Background, Related to Figure S1

stage	wt/wt	wt/cys	cys/cys	resorption	total
E9.5	5 (21.7%)	14 (61.9 %)	4 (17.4%)	0	23 (100%)
E10.5	9 (33.3%)	13 (48.3%)	5 (18.4%)	1	27 (100)
E11.5	8 (28.6%)	16 (57.1%)	4 (14.3)	3	28 (100%)
E12.5	2 (25%)	5 (62.5%)	1 (12.5%)	2	8 (100%)

Embryos obtained from heterozygous *Gpx4*^{cys/wt} breedings (on a *C57BL/6J* genetic background) were isolated at different times of gestation ranging from E9.5-E12.5. Intrauterine resorptions increased by E11.5 indicating that homozygous *Gpx4*^{cys/cys} embryos die around E11.5.

Table S2. PCR Primers, Related to Key Resource Table

Oligonucleotides	Sequence (5' - 3')
Ascl (fwd)	AGGAAGGCGCGCCCTCGCCGGAT
Cys-Gpx4 (rev)	TCAGTTTTGCCGCATTGCGAGGCCACGT
Cys-Gpx4 (fwd)	ACGTGGCCTCGCAATGCGGCAAACTGA
Sbfl (rev)	CTTCCTGGCTCCTGCAGGAAGCAAC
Neo_2 (fwd)	GCGATGCCTGCTTGCCGAATATCAT
Neo_2 (rev)	TTGCTACAATCATGGGCCAGACGGA
Gpx4_mut (fwd)	CATGGTCTGCCTGGATAAGTACAGGT
Gpx4_mut (rev)	CTTGGAAGATACACTACACTGTACACTG
Gpx4_1 (fwd)	GTTTAAGGATGGTGGTGGTAACCTGCTAG
Gpx4_2 (fwd)	GTGGTATCATTAGCTTTAGAAT
Gpx4_3 (rev)	ACTTAGCCCATAGTCCTAAGATCAC
Gpx4_4 (rev)	CTCCCTACCCGGTAGAATTAGCTTG
Trsp (fwd)	GGCGCTATGCAAATGAAGCTAC
Trsp (rev)	GAGCCGGAGTGAACAAATGAACA
p442_Gpx4 (fwd)	CCGGTCAATCAAGCTTATCGATACCGTCGACGGATCCTTGGATCCA CTAGTAACGGC
p442_Gpx4 (rev)	TACGTAACCGGTCTCGAGACGCGTTCTAGAGAATTCTTCGTCTAGAGC TAGCCTAGGC
pRTS1_Gpx4 (fwd)	CCTCCGCGGCCCGAATTCCTGCAGATTTAAATACTAGTGGATCCCCGCGGTTTCGAAACTA GTAACGGCCGCCAGTG
pRTS1_Gpx4 (rev)	CATGCTGGATCCTCTAGAAGTAGGTCGACAGATCTTCTAGAGCTAGCCTAGGC
KIM-1 (fwd)	TCAGCTCGGGAATGCACAA
KIM-1 (rev)	TGGTTGCCTTCCGTGTCTCT
TIMP-2 (fwd)	CAGACGTAGTGATCAGAGCCAAA
TIMP-2 (rev)	ACTCGATGTCTTTGTCAGGTCC
IGFBP7 (fwd)	AAGAGGCGGAAGGTAAAGC
IGFBP7 (rev)	TGGGGTAGGTGATGCCGTT-
18sRNA (fwd)	GCAATTATCCCATGAACG
18sRNA (rev)	AGGGCCTCACTAAACCATCC

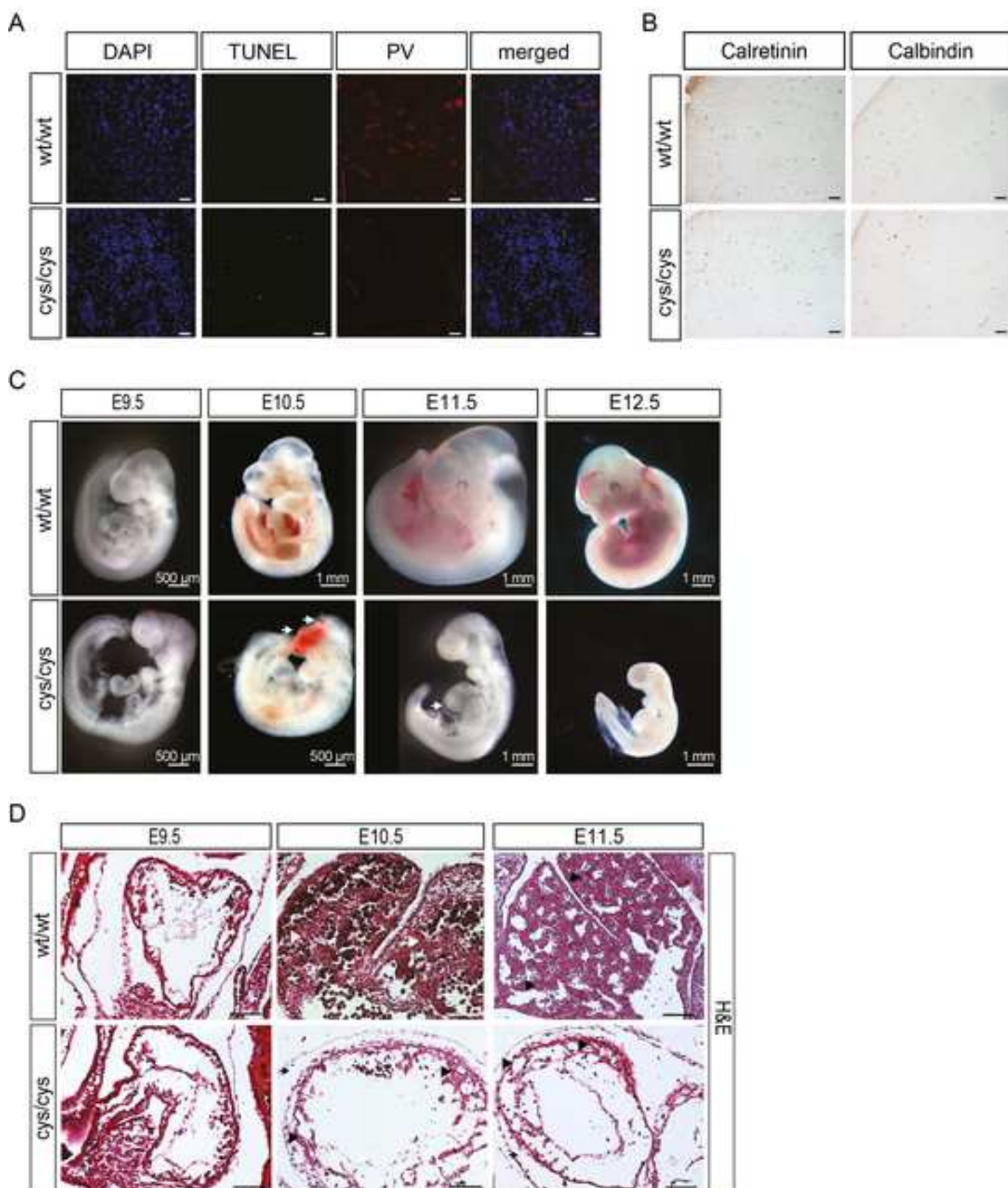
Figure S1

Figure S2

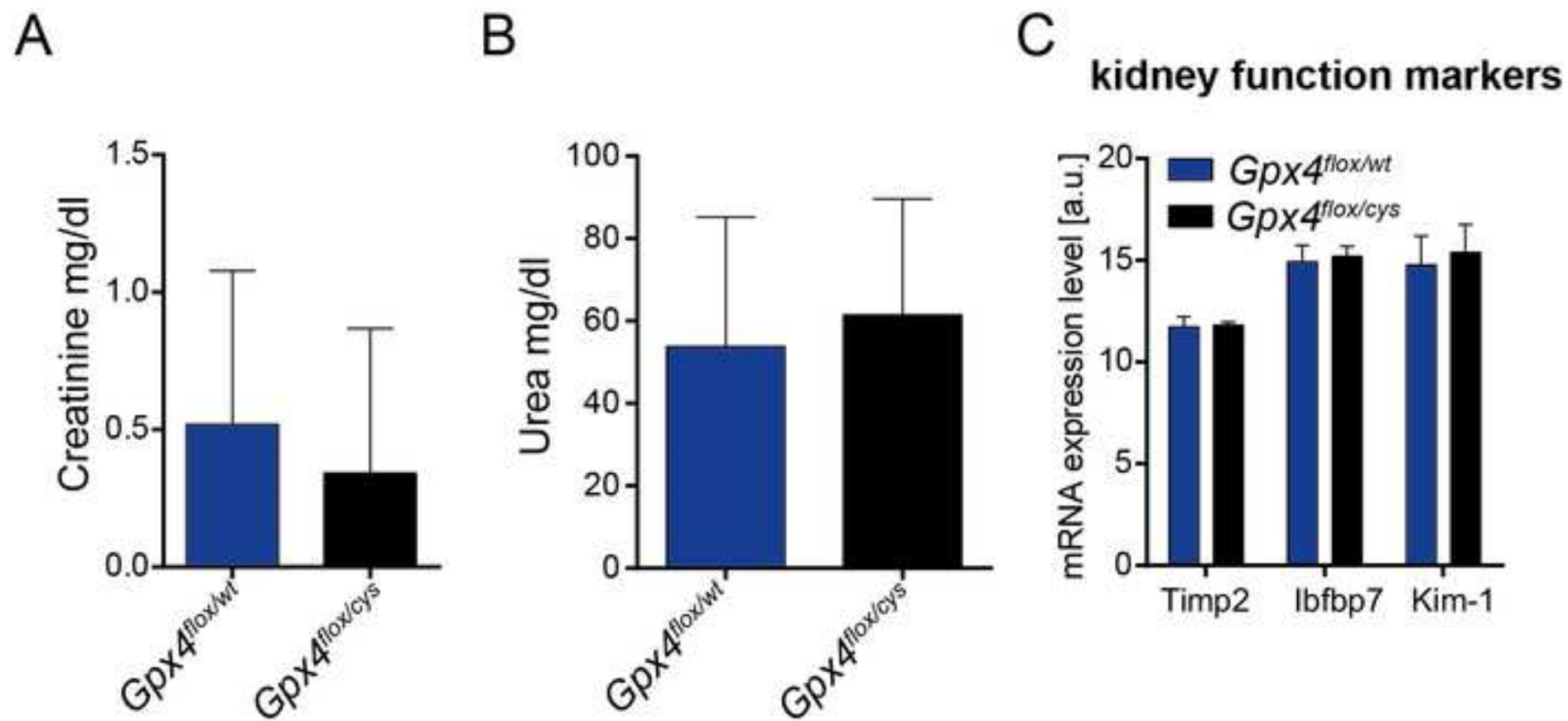


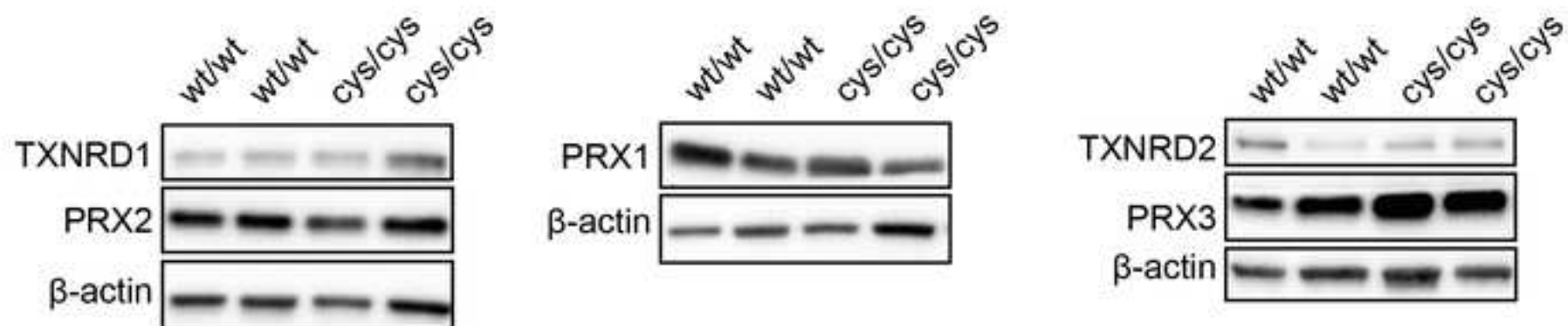
Figure S3

Figure S4

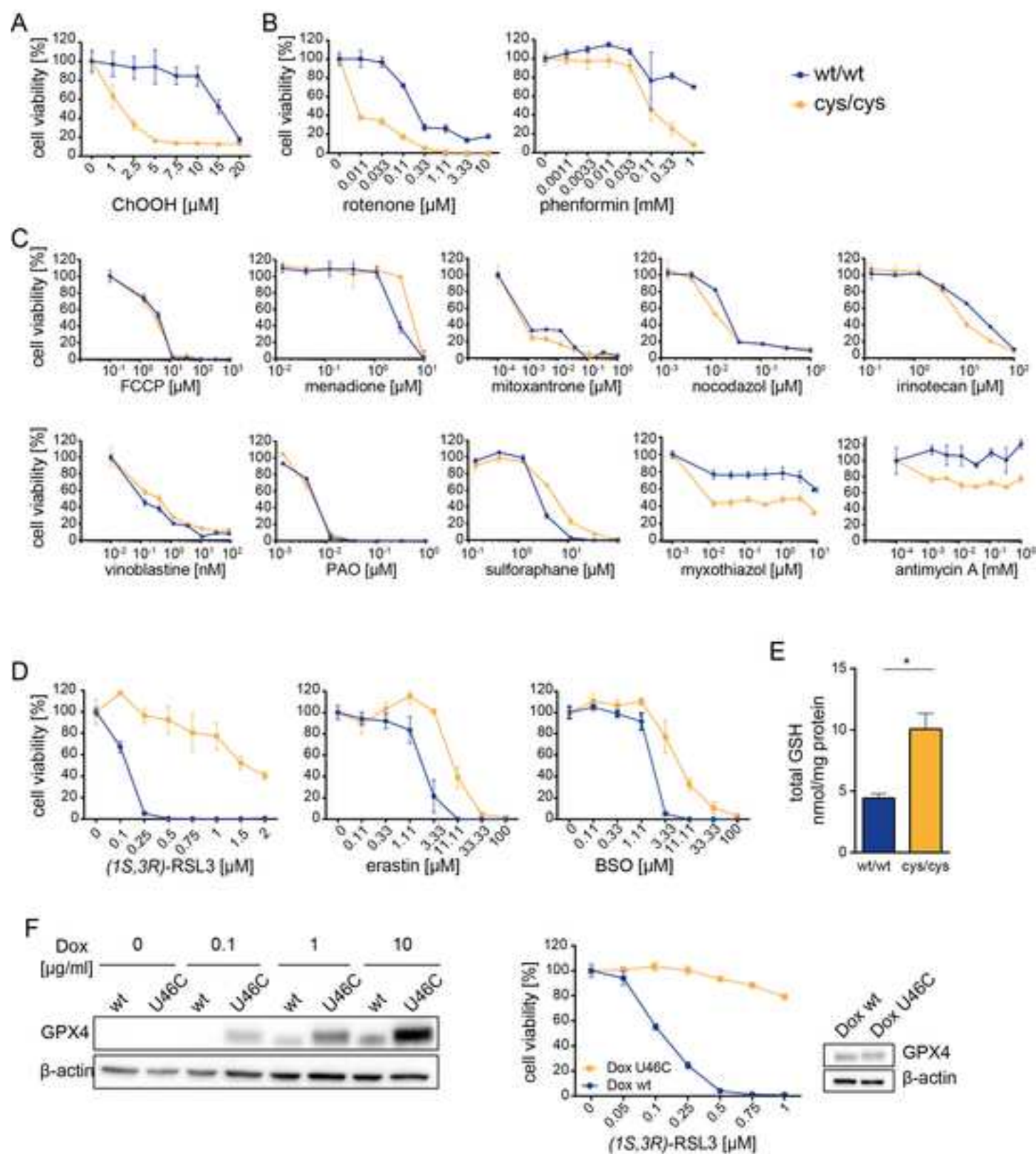


Figure S5

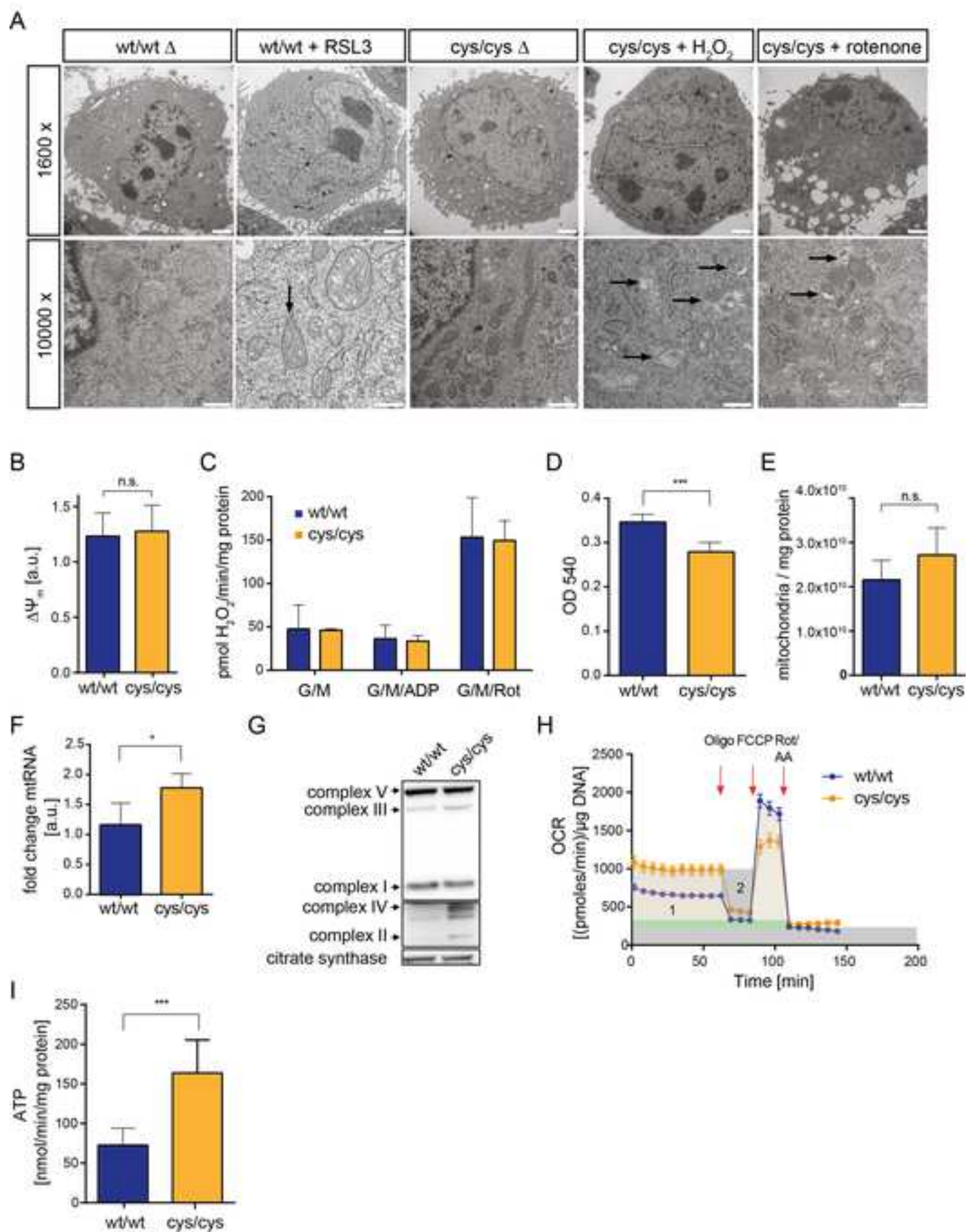
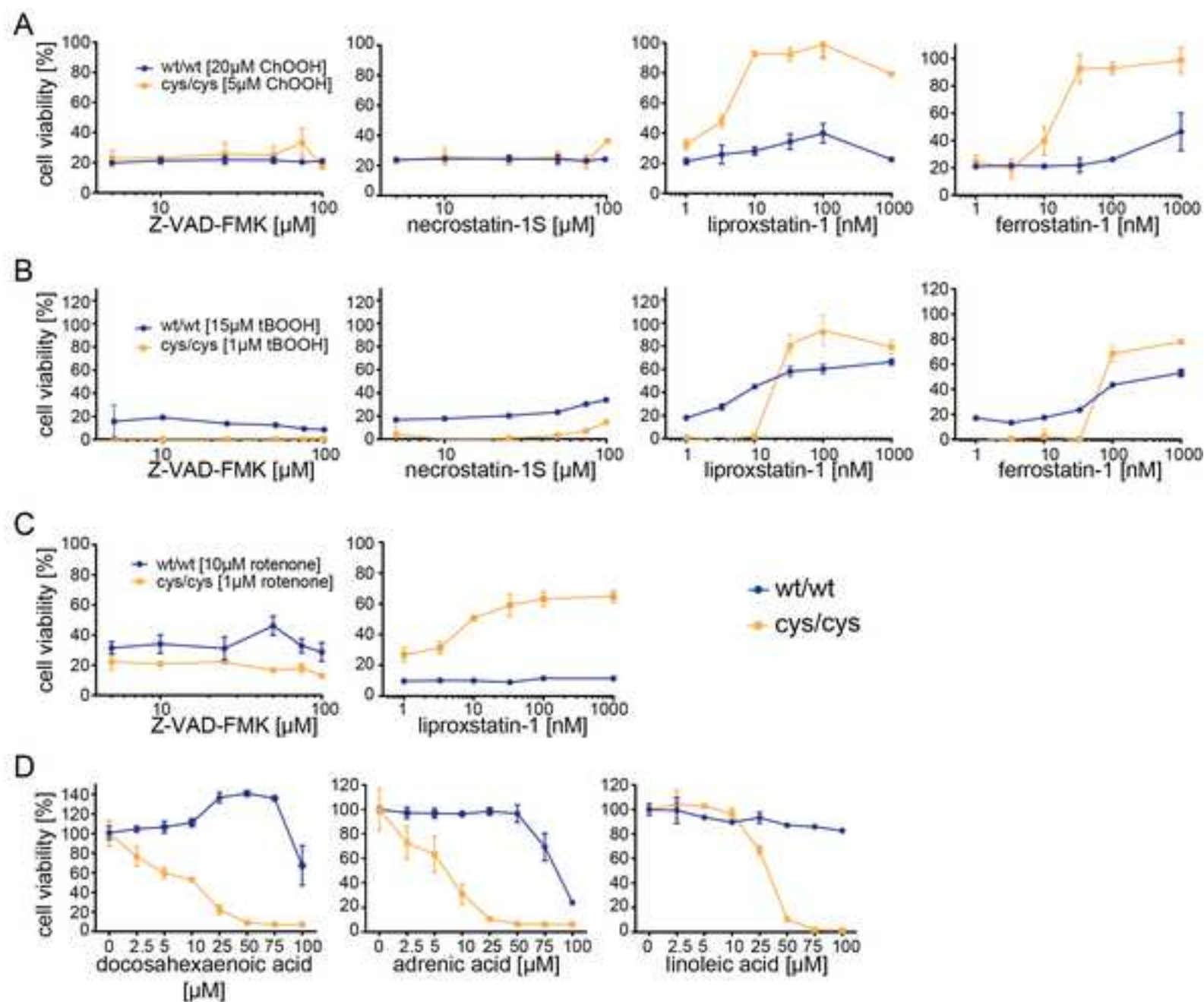


Figure S6



```

H. sapiens      1  MSLGRLCRLKLPALLCGALAAPGLAGTMCASRDD-----WRCARSMHEFSAKDIDGHM
M. musculus    1  MSWGRLSRLKLPALLCGALAAPGLAGTMCASRDD-----WRCARSMHEFSAKDIDGHM
S. lalandi     1  -----MRPLHVFFIFGAVASSGVLLAMSAPTED-----WQTATSIYDFSATDIDGNE
G. gallus      1  -----MCAQADE-----WRSATSIYDFHARDIDGRD
C. virus       1  -----MDDD-----WILKHNIYGFNINLINGKN
T. brucei brucei 1  -----MSTIFDFEVLADADHKP
A. thaliana    1  -----MGASA-----SVPERSVHQFTVKDSSGKD
C. elegans     1  MA-----SNSLLTLAVSFTVILFAPCVEVDDTLRWKQCAVTNQSVFDFQIETLKGDY

                *
H. sapiens     54  VNLDKYRGFVCIITNVASQUGKTEVNYTQVLVDLHARYAECGLRILAFPCNQFGKQEPGSN
M. musculus    54  VCLDKYRGFVCIITNVASQUGKTEVNYTQVLVDLHARYAECGLRILAFPCNQFGRQEPGSN
S. lalandi     48  VSLDRYRGDVVITNVASKUGKTPVNYSQFAQMHAKYAERGLRILAFPSNQFGNQEPGNE
G. gallus      27  VSLEQYRGFVCIITNVASKUGKTAVNYTQVLVDLHARYAECGLRILAFPCNQFGKQEPGDD
C. virus       24  FKLSAYKDRICLFDVNVASECQLADKNYKELTELYSKYFYDGLRIMAFPCNQFGKQEPGNK
T. brucei brucei 17  YNLVQHKGSPLLIYNVASKCGYTKGGYETATALYNKYKSGFTVLVFPNEFGQEPGNE
A. thaliana    25  LNMSIYQGVLLIYNVASKCGFTETNYTQLTELYRKYKQDFEILAFPCNQFLYQEPGTS
C. elegans     53  TDLSQYRGKVTLLVNVATFCAYTQ-QYTDENPILDKYQKQGLVIAAFPCNQFYLQEPDEN

H. sapiens     114 EEIKEFAAGY--NVKFDMPFSKICVNGDDAHPLWKWMKIQPKGKGL-GNAIKWNFTKFLI
M. musculus    114 QEIKEFAAGY--NVKFDMYSKICVNGDDAHPLWKWMKVQPKGRGML-GNAIKWNFTKFLI
S. lalandi     108 SQIKQFAQSY--NAQFDMPFSKINVNGANAHPLWKWLKEQPNGRGFL-GSSIKWNFTKFLI
G. gallus      87  AQIKAFAGY--GVKFDMPFSKIEVNGDGAHPLWKWLKEQPKGRGTL-GNAIKWNFTKFLI
C. virus       84  KEIMNTLKKY--SVLFDVSEKVLVNTIYAHPLWKWLQTRAA-LGDI-AGPIRWNFCKFLI
T. brucei brucei 77  EEIKEFVCTKFK-AEFPIMAKINVNGENAHPLYEYMKKT--KPGILATKAIKWNFTSFLI
A. thaliana    85  QEAHEFACERFK-AEYVPVQKVRVNGQNAAPIYKFLKAS--KPTFL-GSRIKWNFTKFLV
C. elegans     112 HELLNGLTHVRPGN-----G-----

H. sapiens     171 DNGCVVKRYGPMEEPLVIEKDLPHYF-----
M. musculus    171 DNGCVVKRYGPMEEPLVIEKDLPCYL-----
S. lalandi     165 NREGQVVKRYGPLDDPSVVEKDLPOYL-----
G. gallus      144 NREGQVVKRYSPMEDPYVIEKDLPAYL-----
C. virus       140 SPMGYVIKRYDPVINPMSIENDIKKVIQRDNEEMVLNRWVVPDTPCSEDNNKIPGDVY
T. brucei brucei 134 DRDGVVVERFSPGASVKDIEEKLIPLLESTQSA-----
A. thaliana    141 GKDGLVIDRYGTMVTPLSIEKDIKKALEDA-----
C. elegans     127 -----

```



[Click here to access/download](#)

Supplemental Movies and Spreadsheets
46CA.mp4

